Journal of Marine Systems 251 (2025) 104109

Contents lists available at ScienceDirect

Journal of Marine Systems

journal homepage: www.elsevier.com/locate/jmarsys

# Comparing *in situ* and satellite-derived primary production estimates in the Canary Current upwelling region

Nauzet Hernández-Hernández [a,*], Yeray Santana-Falcón [a,b], María F. Montero [a], Mar Benavides [c,d,e], Antonio Delgado-Huertas [f], Xosé A. Álvarez-Salgado [g], Peter Land [h], Javier Arístegui [a,*]

[a] *Instituto de Oceanografía y Cambio Global, IOCAG, Universidad de Las Palmas de Gran Canaria ULPGC, Las Palmas, Spain*
[b] *CNRM, Université de Toulouse, Météo-France, CNRS, Toulouse, France*
[c] *National Oceanography Centre, European Way, Southampton SO14 3ZH, United Kingdom*
[d] *Aix Marseille Univ., Université de Toulon, CNRS, IRD, MIO UM 110, 13288 Marseille, France*
[e] *Turing Center for Living Systems, Aix-Marseille University, 13009 Marseille, France*
[f] *Instituto Andaluz de Ciencias de la Tierra (IACT-CSIC-UGR), Armilla, Spain*
[g] *CSIC - Instituto de Investigacións Mariñas (CSIC-IIM), Vigo, Spain*
[h] *Plymouth Marine Laboratory, Plymouth, United Kingdom*

A R T I C L E I N F O

*Keywords:*
Phytoplankton biomass
Photosynthetic parameters
Primary production methods
Primary production models
Canary current EBUS

A B S T R A C T

Satellite-based Net Primary Production (NPP) estimates are arguably the best way to improve our understanding of large-scale ocean productivity and to validate Earth System Models. Despite significant progress over recent decades, satellite-derived NPP estimates still suffer from large uncertainties, primarily due to the limited number of *in situ* primary production (PP) measurements available for their validation. In addition, the most widely used algorithms lead to different, sometimes even contradictory, results. Along with measurements of chlorophyll *a* concentration (Chl*a*) and phytoplankton biomass ($C_{phyto}$), here we present *in situ* measurements of PP using $^{14}C$ uptake and $^{13}C$ isotope tracing, as well as $O_2$ and $^{18}O_2$ evolution inside incubation bottles, across the transition zone from the coastal Canary Eastern Boundary Upwelling System (CanEBUS) to the open ocean waters of the Cape Verde Frontal Zone (17–23°N; 16–26°W). We also calculate assimilation numbers ($P^b_{opt}$) and growth rates (μ) from *in situ* measurements. First, we compared *in situ* PP estimates measured concurrently using the four abovementioned techniques. We then tested the performance of four widely-used models including the Vertically Generalized Production Model (VGPM) and its variant based on Eppley's description of the growth function (Eppley), the Carbon-based Productivity Model (CbPM), and the Carbon, Absorption and Fluorescence Euphotic-resolving model (CAFE), along with the satellite-derived input variables that feed these algorithms. We found that the Chl*a*-based VGPM and Eppley models were significantly correlated with *in situ* estimates, regardless of the satellite source used as input data. As for models based on $C_{phyto}$, only the CbPM from the Visible Infrared Imaging Radiometer Suite (VIIRS) data demonstrated performance comparable to that of the Chl*a*-based models. In all other cases, $C_{phyto}$-based models were uncorrelated with *in situ* PP estimates. Our results indicate that the bias associated with the VGPM and Eppley models is primarily due to the algorithms' inability to accurately assess $P^{opt}_b$ . Meanwhile, the retrieval of both satellite-derived $C_{phyto}$ and μ leads to a poor estimate of NPP by the CbPM. Our findings suggest that enhancing the accuracy of NPP estimates derived from satellite-based models necessitates the refinement of the methodology employed in deriving the input data and their subsequent validation, rather than developing increasingly complex models.

* Corresponding authors.
*E-mail addresses:* nauzet.hernandez@ulpgc.es (N. Hernández-Hernández), javier.aristegui@ulpgc.es (J. Arístegui).

https://doi.org/10.1016/j.jmarsys.2025.104109
Received 7 January 2025; Received in revised form 15 July 2025; Accepted 16 July 2025
Available online 20 July 2025

## 1. Introduction

Few ecosystems on Earth play as significant an ecological, climatological, and socio-economic role as the Eastern Boundary Upwelling Systems (EBUS's; Kämpf and Chapman, 2018). Despite comprising less than 3 % of the total ocean area, wind-driven upwelling of cold, nutrient-rich waters along EBUS contributes to approximately 10 % of global phytoplankton biomass production (Carr, 2002; Lachkar and Gruber, 2012; Messié and Chavez, 2015), supporting about 20 % of the global fish catch (FAO, 2022; Pauly and Christensen, 1995; Pauly and Zeller, 2016). Furthermore, these regions are important biodiversity hotspots, hosting various marine mammals and migrant seabirds, and supporting a lucrative eco-tourism industry (Arístegui et al., 2009; Block et al., 2011; Fréon et al., 2009; Kämpf and Chapman, 2018). The goods and services provided by EBUS are estimated to benefit around 80 million people living along their coastal regions, with an economic value of approximately half a billion euros (FAO, 2022; García-Reyes et al., 2015; Levin and Le Bris, 2015). Understanding the spatial and temporal variability of the EBUS productivity, as well as the potential effects of climate change on their ecological functioning, is closely linked to the study of primary production (PP; Barange et al., 2014; Blythe et al., 2020; Kulk et al., 2020). However, the large spatial and temporal scales, along with the heterogeneity of EBUS in terms of productivity, complicate the study of PP in these systems (Arístegui et al., 2009; Basterretxea and Arístegui, 2000).

Measuring PP in marine waters relies on time-consuming temperature and light-controlled incubations in which oxygen and carbon production are typically measured over a period of 24 h. Most common techniques are based on radiolabeled $^{14}$C-uptake and Winkler-based oxygen measurements (Carpenter, 1965; Steeman-Nielsen, 1952). Additional methods include using stable isotopes like $^{18}O_2$ (Bender et al., 1987) and $^{13}$C (Slawyk et al., 1977), measuring variations in the isotopic composition of dissolved $O_2$ and Ar ratios (Luz and Barkan, 2011), and active fluorescence (Kolber and Falkowski, 1993). Despite the latter being less time-consuming, the $^{14}$C and $O_2$ methods remain the gold standard.

While these methods have contributed to significant global datasets, the coverage is still insufficient to accurately study large, heterogeneous ecosystems like the EBUS (Bouman et al., 2018; Mattei and Scardi, 2021). Moreover, all these techniques often yield different results, impeding comparisons between methods and thus limiting the spatial and temporal coverage of the data (Fahey and Knapp, 2007). Although attempts to reconcile these discrepancies have been proposed (Arístegui et al., 1996; Arístegui and Harrison, 2002; López-Sandoval et al., 2018; Lottig et al., 2022; Regaudie-de-Gioux et al., 2014; Sanz-Martín et al., 2019), they remain a subject of ongoing debate (Marra, 2012; Quay et al., 2010). Hence, a larger spatiotemporal coverage of high-quality *in situ* PP measurements is critical for validating satellite-based net primary production (NPP) models.

The development of satellite-based NPP estimates marked a significant breakthrough in the study of large-scale ecosystems, as they overcome the spatial and temporal limitations of *in situ* methods. These remotely sensed NPP estimates are computed using satellite-derived data on phytoplankton biomass -either chlorophyll *a* (Chl*a*) or phytoplankton carbon ($C_{phyto}$)- which are converted into organic carbon production rates by means of algorithms. These algorithms, or models, are then validated against *in situ* PP data (Groom et al., 2019; Lee et al., 2015; Westberry et al., 2023). The models are based on long-established relationships between the photosynthetic process, Chl*a* and light availability (Platt and Sathyendranath, 1988; Platt and Lewis, 1987; Ryther, 1956; Ryther and Yentsch, 1957).

Despite decades of effort, satellite-derived NPP estimates remain far from satisfactory. Discrepancies between *in situ* and satellite-derived PP estimates can be as large as two to three times, regardless of temporal or spatial scales (*e.g.*, Campbell et al., 2002; Carr et al., 2006; Friedrichs et al., 2009). Comparisons among models have also produced different, and sometimes even contradictory, results (Campbell et al., 2002; Carr et al., 2006; Friedrichs et al., 2009; Gómez-Letona et al., 2017; Saba et al., 2011). In fact, the IPCC Special Report on the Ocean and Cryosphere in a Changing Climate assigns a low confidence level to satellite-based marine PP trends (Bindoff et al., 2022).

The inaccuracies of NPP models become more pronounced in EBUS, where the ocean's most productive and least productive regions converge. These regions require the simultaneous study of contrasting surface bio-optical properties and water column structures. Therefore, resolving the sources of discrepancies between *in situ* and satellite-derived model inputs -such as Chl*a*, $C_{phyto,}$ assimilation numbers ($P^b$), or growth rate (μ)- and outputs like NPP is crucial for improving model accuracy (Brewin et al., 2021; IPCC, 2022).

Our objectives are twofold. First, we aim to reconcile the most widely used *in situ* methodologies for measuring PP; and second, we evaluate the performance of four widely used satellite-based PP models, to identify the most suitable option for studying highly contrasting ecosystems such as EBUS. This study significantly advances our understanding of the complex relationships between various methods of estimating PP in the ocean, including *in situ* techniques and remote sensing. Notably, this study stands as the sole published dataset that has measured these relationships simultaneously through the application of four predominant techniques, as far as we know.

## 2. Methods

### 2.1. Sampling collection and incubation

The *in situ* data for this study was obtained during the FLUXESI cruise, from July 10 to August 11, 2017, onboard the R/V Sarmiento de Gamboa. A grid of 35 stations spanning the Coastal Transition Zone of the Mauritanian part of the Canary Eastern Boundary Upwelling System (CanEBUS) was sampled (Fig. 1). At each station, CTD (Sea-Bird CTD 911+, Sea-Bird Scientific, USA) casts were performed down to the seafloor. At 11 of the 35 stations, water samples were collected for PP measurements using a General Oceanics rosette sampler equipped with 24 Niskin bottles of 12 L (Fig. 1). Samples for *in situ* primary production (PP) measurements were directly poured from Niskin bottles using a silicone tube with a 280 μm mesh attached to its end to remove predators from three depths: surface, above the Deep Chlorophyll Maximum (DCM), and at the DCM. After water collection, the samples were placed in incubators. Three on-deck methacrylate incubators were used, simulating the *in situ* light and temperature conditions corresponding to the different sampling depths. Natural light was attenuated using blue foil screening (172 Lagoon Blue foil, Lee filters, USA) according to light profiles obtained at each station with a Photosynthetically Active Radiation (PAR) sensor (Li-COR/Biospherical, LICORbio, USA) attached to the CTD rosette. Given that the three depths at which PP was measured were within the mixing layer, the differences in temperature were minimal. This made it impossible to reproduce these differences using water chillers. Consequently, surface water was circulated through the three incubators to control the temperature. All samples were incubated for 24 h, with their positions arranged in the incubators to minimize shadowing as much as possible.

### 2.2. In situ data

#### 2.2.1. Primary production

To estimate $^{14}$C-based PP rates, four 70 mL water samples were collected in tissue culture treated flasks of 25 cm$^2$ of growth area (Sarstedt, Germany). Each sample was spiked with 15 μCi of $^{14}$C-labelled sodium bicarbonate solution ($NaH^{14}CO_3$; >99 atom %, Perkin Elmer, USA). One of the four samples was covered with opaque foil to shield it from light during incubation, allowing for the measurement of dark carbon uptake. Afterward, the entire sample was filtered under low vacuum pressure onto a 0.2 μm pore-size 25 mm ø polycarbonate filter

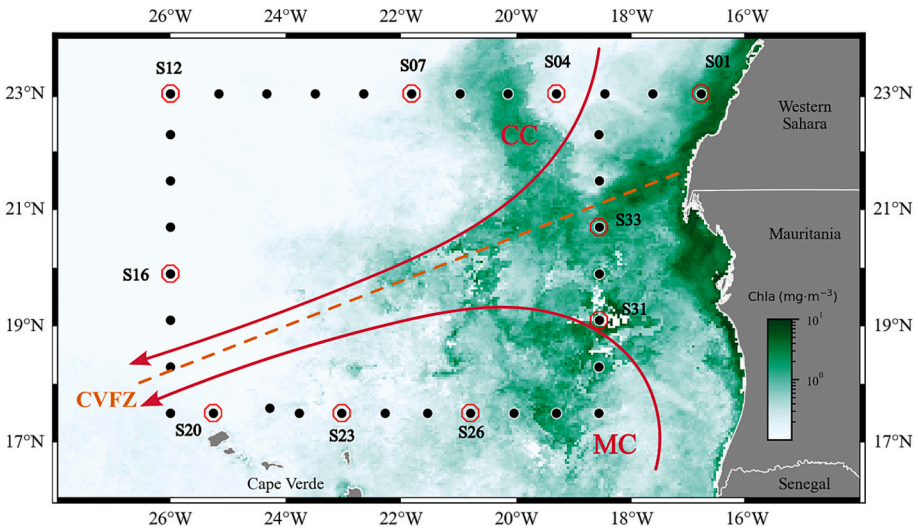


**Fig. 1.** Oceanographic stations sampled during the FLUXES I cruise, superimposed on a map of monthly-averaged surface chlorophyll *a* (Chl*a*, mg·m$^{-3}$) for July 2017. Stations where primary production samples were collected are highlighted with red circles. The Chl*a* data is part of the Ocean Colour Climate Change Initiative (OC-CCI) and was downloaded from the "PRIMary-productivity in Upwelling Systems (PRIMUS)" project site (https://primus.eofrom.space). CC: Canary Current; MC: Mauritanian Current; CVFZ: Cape Verde Frontal Zone. (For interpretation of the references to colour in this figure legend, the reader is referred to the web version of this article.)

(Whatman, Merck, Germany) using a circular manifold (Oceomic, Fuerteventura, Canary Island, Spain) designed for collecting the filtrate. The filters were then placed in 10 mL scintillation vials. Five mL of the filtrate were place in 20 mL scintillation vials, acidified with 100 μL of 17.5 % HCl and placed in an orbital oscillator for 24 h, while the filters were exposed to 37 % HCl fumes for the same duration. Finally, 10 mL and 5 mL of Ultima Gold XR scintillation cocktails were added to the 20 mL and 10 mL vials, respectively, thoroughly mixed, and stored in darkness for 24 h. Isotopic disintegrations per minute were measured using a Beckman LS-6500 scintillation counter (Beckman Coulter, USA). Primary production rates (in mmol C·m$^{-3}$·d$^{-1}$) were calculated according Hernández-Hernández et al. (2018). The primary production rates obtained from the filters corresponded to particulate primary production (PO$^{14}$C), while rates from the filtrate represented dissolved primary production (DO$^{14}$C; not shown here). Total primary production (TO$^{14}$C) was calculated as the sum of DO$^{14}$C and PO$^{14}$C.

For $^{13}$C-based PP estimations, 4.5 L polycarbonate bottles (Nalgene, Thermo Fisher Scientific, USA), previously cleaned with 10 % HCl, were filled with water samples in triplicates, ensuring no bubbles were present. One of the three samples was immediately filtered to determine the $^{13}$C background enrichment of particulate carbon. The remaining two samples were inoculated with 500 μL of 500 mM $^{13}$C-labelled sodium bicarbonate (NaH$^{13}$CO$_3$; >98 atom %, Sigma Aldrich, USA) and incubated for 24 h. All samples were gently filtered onto precombusted 25 mm ø GF/F filters (Whatman, Merck, Germany). The filters were dried on board at 50 °C for 24 h and stored in silica gel desiccant until analysis in land-based laboratories. The percentage of $^{13}$C atoms was measured using a Thermo Flash 1112 elemental analyzer interfaced with a Conflo III connected to a Thermo Delta V Advantage isotope ratio mass spectrometer (Thermo Fischer Scientific, USA). Finally, PP rates (PO$^{13}$C, mmol C·m$^{-3}$·d$^{-1}$) were calculated following the method outlined by Hama et al. (1993). It should be noted that $^{13}$C-based PP rates were measured alongside $^{15}N_2$ fixation rates. For details of the complete procedure see Hallstrøm et al. (2022).

For PP estimations based on the evolution of oxygen concentration during the incubation period, 4 L bottles were filled with water sample and maintained inside the corresponding incubators to avoid temperature changes during subsampling. 12 calibrated 125 mL BOD bottles were filled using silicone tubes to allow for sample overflow, ensuring a final bubble-free state after closing. Four of the 12 bottles, referred to as 'initials', were immediately fixed by sequentially adding 1 mL of manganese sulfate ($MnSO_4$), and 1 mL of sodium iodide-sodium hydroxide (NaI + NaOH) alkaline solution. These bottles were then stored submerged in seawater under dark conditions. The remaining bottles were placed in incubators for 24 h, with half of them (four bottles) covered with light proof bags ('dark') and the other four left uncovered ('light'). After incubation, the 'dark', and 'light' samples were fixed following the same procedure as the 'initials' and allowed to sediment the precipitate for at least 4 h. Finally, all samples were acidified with 1 mL of 5 M sulphuric acid ($H_2SO_4$) just prior to analysis using an automated, precise titration system with colorimetric end-point detection (SiS DOA, GmbH, Germany) following the Winkler technique and the recommendations of Bryan et al. (1976), and Hansen (1999). Net community production (NCP, mmol $O_2$·m$^{-3}$·d$^{-1}$) rates were calculated as the difference between the 'light' and 'initial' bottles; community respiration (CR, mmol $O_2$·m$^{-3}$·d$^{-1}$) was calculated as 'initials' minus 'dark' bottles (not shown here); and gross primary production (GPP, mmol $O_2$·m$^{-3}$·d$^{-1}$) was determined as the sum of NCP and CR. The disparities among replicates were seldom greater than 2 mmol $O_2$·m$^{-3}$, with a standard deviation ranging from 0.075 to 2.427 and a mean standard error < 0.1 mmol $O_2$·m$^{-3}$. Replicates demonstrating discrepancies surpassing 3 mmol $O_2$·m$^{-3}$ were systematically excluded from the analysis.

For $^{18}$O-based PP measurements, seawater samples were distributed into eight borosilicate vials (12 mL) designed to allow overflow, preventing atmospheric contamination. Half of the vials (four vials) were immediately poisoned for the determination of natural $\delta^{18}O$ by adding 100 μL of saturated mercury chloride ($HgCl_2$) and storing them in the darkness. The other four vials were spiked with 80 μL of $H_2^{18}O$ (>98 atom %) and gently mixed before being incubated for 24 h. After incubation, all vials were fixed following the previously mentioned procedure and stored in the darkness until analysis at the land-based Stable-Isotope Laboratory of IACT-CSIC in Armilla, Spain. Prior to analysis, the samples were diluted to avoid contamination of the analyzer (~1:20) with a laboratory standard of known isotopic composition. The $\delta^{18}O$ composition of the samples was measured using a liquid water isotope analyzer (Los Gatos Research, USA). The $^{18}$O-based PP rates, expressed in mmol $O_2$·m$^{-3}$·d$^{-1}$, were calculated following the methods outlined by Bender et al. (1999). The precision of the $^{18}O_2$ technique demonstrated a high degree of similarity to that of the $O_2$ method, with differences among replicates generally less than 2 mmol $O_2$·m$^{-3}$ (sd: 0.025–2.123; se: <0.1

mmol $O_2 \cdot m^{-3}$).

A photosynthetic quotient (PQ = moles $O_2$ released / moles C fixed) of 1.4 (Trentman et al., 2023) was used to convert oxygen to carbon units in order to compare with satellite-derived PP estimates. Depth-integrated *in situ* PP rates (mg $C \cdot m^{-2} \cdot d^{-1}$) were calculated by employing the trapezoidal rule on the surface-to-DCM profiles of volumetric rates.

#### 2.2.2. Chlorophyll *a*

Five hundred mL of water was gently filtered onto 0.2 μm pore-size 25 mm ø polycarbonate filter (Whatman, Merck, Germany) under low vacuum pressure using a flat filtration manifold. The Chl*a* collected on the filters was extracted in 10 mL of 90 % *v*/v acetone and stored at −20 °C for 24 h. Chl*a* concentration (mg Chl$a \cdot m^{-3}$) was then measured fluorometrically using a previously calibrated Turner 10-AU bench fluorometer (Turner Designs, USA), following the method of Holm-Hansen et al. (1965).

#### 2.2.3. Phytoplankton biomass

Pigmented picoplankton (0.2–2 μm) and nanoplankton (2-20 μm) cells were counted using a FACScalibur (Becton and Dickinson, USA) flow cytometer. Samples for picoplankton (1.6 mL) and nanoplankton (3.2 mL) counts were collected in cryovials of 2 and 4 mL, respectively, fixed with paraformaldehyde to a final concentration of 2 %, incubated at 4 °C during 30 min prior flash-frozen in liquid nitrogen, and stored at −80 °C until analysis in the land-based laboratories in Gran Canaria, Canary Islands. For picoplankton counts, a suspension of yellow-green 1 μm ø latex beads (~$10^5$ bead$\cdot mL^{-1}$, Polysciences, USA) was added as an internal standard, and samples were run at 75 μL$\cdot min^{-1}$ for 150 s. For nanoplankton, red 2 μm ø latex beads (~$10^5$ bead$\cdot mL^{-1}$, Polyscience, USA) were used as the internal standard, and samples were run at 170 μL$\cdot min^{-1}$ for 300 s. Picoplankton and nanoplankton groups were identified based on their side-scatter (SSC) *vs* red (FL3), and orange (FL2) fluorescence signatures in bivariate plots. Water samples (250 mL) for autotrophic microplankton (20–200 μm) counting and identification were stored in brown glass bottles and immediately fixed with alkaline Lugol's iodine (1 % final concentration). Back in the lab, subsamples (100 mL) were sedimented for at least 24 h in 100 mL Utermöhl chambers before being counted using an inverted microscope IX83 (Olympus, Japan) following Utermöhl (1931).

To estimate cell-sizes of picoplankton and nanoplankton, the flow cytometer was calibrated using non-fluorescent latex beads of 0.5, 1, 2, 4, 6, 10 and 15 μm in diameter (Molecular Probes, USA). The SSC values of the calibration beads were normalized to the SSC measured for the fluorescence standard beads added to each sample (1 μm for picoplankton and 2 μm for nanoplankton settings). Linear regression was performed between bead diameters and normalized SSC for picoplankton (ø = 9.914·log SSC - 0.219; $r^2 = 0.92$) and nanoplankton (ø = 4.753·log SSC + 0.008; $r^2 = 0.93$). Cell diameters (μm) were inferred from the relative SSC of each group and used to calculate cell biovolume ($\mu m^3$), assuming spherical shapes. Biomass was estimated using conversion factors: 240 fg C$\cdot \mu m^{-3}$ for *Prochlorococcus*, 230 fg C$\cdot \mu m^{-3}$ for *Synechococcus*; 237 fg C$\cdot \mu m^{-3}$ for picoeukaryotes (Bjørnsen, 1986); and 220 fg C$\cdot \mu m^{-3}$ for nanoeukaryotes (Børsheim and Bratbak, 1987). Microplankton cell volumes were obtained from Olenina et al. (2006), and volume-to-carbon biomass was converted using equations from Menden-Deuer and Lessard (2000). Phytoplankton biomass ($C_{Phyto}$) was calculated as the sum of the biomass of all groups.

#### 2.2.4. Assimilation numbers and growth rates

Hourly $TO^{14}C$ rates measured at each depth were normalized to *in situ* Chl*a* to calculate the assimilation numbers ($P^b$; mg C· mg Chl$a^{-1} \cdot h^{-1}$). The highest $P^b$ value at each station was defined as $P^b_{opt}$ (Behrenfeld and Falkowski, 1997a). To estimate phytoplankton growth rates (μ; $d^{-1}$), daily $TO^{14}C$ rates were normalized to $C_{phyto}$. The highest μ value measured in the water column was selected for testing satellite-based products (Laws, 2013).

### 2.3. Remote sensing data

#### 2.3.1. Primary production models

We selected four well-known, easily accessible, and broadly used PP models for comparison. They are briefly presented below.

(1) The Vertically Generalized Production Model (VGPM) was described by Behrenfeld and Falkowski (1997b). This model is based on the dependence of PP on Chl*a*. A Chl*a*-specific assimilation term ($P^b_{opt}$) is employed to transform a standing stock, such as Chl*a*, into a NPP rate. $P^b_{opt}$ is defined by 7th degree polynomial function dependent on sea surface temperature (SST). Additionally, a volume function is derived based on the depth of the euphotic layer ($Z_{Eu}$) and on the daily ($L_{day}$) and vertical variation of PAR (f (PAR)), which is then used to obtain depth-integrated NPP estimates.

$$NPP = Chla \cdot P^b_{opt} \cdot L_{day} \cdot f(PAR) \cdot Z_{Eu}$$

(2) The modified version of the VGPM (Eppley) differs from its predecessor in the manner in which $P^b_{opt}$ is described. Instead of using a polynomial function, the Eppley model employs the exponential expression described by Morel (1991). This function is based on the dependence of the growth function on SST described by Eppley (1972).

(3) The Carbon-based Productivity Model (CbPM) was first described by Behrenfeld et al. (2005) and subsequently updated by Westberry et al. (2008). This model uses carbon ($C_{Phyto}$) instead of Chl*a* as a proxy for phytoplankton biomass, and growth rates (μ) dependent on the C:Chl*a* to transform the carbon stock into a PP rate. Moreover, the revised version of Westberry et al. (2008), no longer utilizes a volume function but instead describes a phytoplankton proxy as a function of depth-dependent photoacclimation (f ($I_g$)).

$$NPP = C_{phyto} \cdot \mu \cdot f(I_g)$$

(4) The Carbon, Absorption and Fluorescence Euphotic-resolving model (CAFE) is the most recently described model (Silsbe et al., 2016). This algorithm diverges from the conventional approach to estimating NPP by employing a phytoplankton biomass proxy and a standing stock to rate transforming term. CAFE utilizes phytoplankton energy absorption ($Q_{PAR}$) and the efficiency ($\varphi_\mu$) with which that energy is transformed into carbon biomass to estimate NPP.

$$NPP = Q_{PAR} \cdot \phi_\mu$$

#### 2.3.2. Data source and resolution

Both NPP and input data were directly downloaded from the open-access Ocean Productivity site of the Oregon State University (OSU, http://science.oregonstate.edu/ocean.productivity/). The input data were obtained from two satellites, the Visible Infrared Imaging Radiometer Suite (VIIRS), and the Moderate Resolution Imaging Spectroradiometer (MODIS). Products were 8-day averaged compositions with a spatial resolution of 4 × 4 km.

### 2.4. Statistical analysis

#### 2.4.1. Data comparisons

To identify differences among the datasets used in this paper, non-parametric Kruskal-Wallis tests were conducted. The null hypothesis -that there are no significant differences between the data being compared- was accepted for *p*-values greater than the significance level ($\alpha = 0.05$), and for H values exceeding the critical value of H ($H_c$) for each case (Kruskal and Wallis, 1952). Potential correlations between log-normalized datasets were assessed using model II (Reduced Major Axis, RMA) linear regressions.

#### 2.4.2. Models' performance assessment

The skill of each model was evaluated by analyzing the total root mean square difference (RMSD, Dorans and Holland, 2000):

$$RMSD = \sqrt{\frac{1}{N}\sum_{i=1}^{N}\Delta(i)^2}$$

where model-data misfit in $\log_{10}$ space ($\Delta$) is defined as:

$$\Delta(i) = log(PP_{sat}(i)) - log(PP_{is}(i))$$

$PP_{sat}$ are the rates estimated by the different models, and $PP_{is}$ are the rates measured by the different *in situ* techniques. RMSD is composed by the bias (B), which represents the difference between the *in situ* and satellite means, and the unbiased RMSD (uRMSD), which represents the difference of variability.

$$RMSD^2 = B^2 + uRMSD^2$$

$$B = \overline{log_{10}(PP_{sat})} - \overline{log_{10}(PP_{is})}$$

$$uRMSD = \sqrt{RMSD^2 - B^2}$$

The closer the values of B, uRMSD, and consequently RMSD are to 0, the better the model's performance and predictive capabilities. The value of B also indicates whether a model consistently underestimates (negative values) or overestimates (positive values) *in situ* data.

Finally, we replaced the model's satellite-estimated input data with *in situ* data when available, reran the models, and compared the results with the original data to assess whether the model limitations were associated with the satellite data or the models themselves. This procedure could not be performed for CAFE, as the required input parameters were not measured *in situ*.

## 3. Results

### 3.1. Comparing in situ PP measurement methods

*In situ* volumetric PP rates spanned three orders of magnitude, except for those measured by $PO^{13}C$ method (Fig. 2a; Table S1). Oxygen-based methods showed higher rates than carbon-based techniques, with mean values of 6.36 ± 12.51, 4.84 ± 9.07, and 3.83 ± 11.55, mmol $O_2 \cdot m^{-3} \cdot d^{-1}$ for $O_2$-GPP, $^{18}O_2$-GPP, and $O_2$-NCP respectively; and 2.95 ± 4.83, 2.35 ± 4.04, and 1.00 ± 0.86 mmol $C \cdot m^{-3} \cdot d^{-1}$ for $TO^{14}C$, $PO^{14}C$, and $PO^{13}C$, respectively (Table S1). The data distribution and ranges among the techniques were quite similar, with $^{18}O_2$-GPP, $PO^{14}C$, and $TO^{14}C$ being the most comparable to each other (Fig. 2a). The $PO^{13}C$ technique showed the lowest mean PP rates and variability, ranging from 0.14 to 2.85 mmol $C \cdot m^{-3} \cdot d^{-1}$ (Table S1). Nevertheless, there were no statistically significant differences among the six techniques as indicated by the Kruskal-Wallis test (*p*-value = 0.08; H = 9.77, $H_c$ = 11.07). Oxygen to carbon ratios ($O_2$:C) also displayed high variability, in some cases up to one order of magnitude (Fig. 2b). Ratios calculated using $O_2$-GPP rates were higher (generally >3) than those obtained with $^{18}O_2$-GPP (1.22–2.18) (Table 1). $O_2$ to $TO^{14}C$ ratios were consistently the lowest, while $O_2$:$PO^{14}C$ and $O_2$:$PO^{13}C$ presented the highest $O_2$:C when compared with $O_2$-GPP and $^{18}O_2$-GPP, respectively. A clear depth gradient was observed in $O_2$:C ratios, with values close to 1 at the surface and increasing with depth up to 6 (Table 1). The same pattern was observed for the $O_2$ to $^{18}O_2$ ratios.

Reduced major axis (RMA) linear regressions of PP rates further emphasize the similarities between PP techniques (Table 2). Excluding the $^{13}C$-uptake method, correlation coefficients ($r^2$) between the various

**Table 1**
Mean (±sd) values for $O_2$ to C ratios, and $O_2$-GPP to $^{18}O_2$-GPP ratios for the surface, above the Deep Chlorophyll Maximum (DCM), and at the DCM.

| Depth | $O_2$-GPP/ $TO^{14}C$ | $O_2$-GPP/ $PO^{14}C$ | $O_2$-GPP/ $PO^{13}C$ | $^{18}O_2$-GPP/ $TO^{14}C$ | $^{18}O_2$-GPP/ $PO^{14}C$ | $^{18}O_2$-GPP/ $PO^{13}C$ | $O_2$ /$^{18}O_2$-GPP |
|---|---|---|---|---|---|---|---|
| Surface | 1.58 ± 1.01 | 2.40 ± 1.42 | 3.16 ± 4.60 | 1.05 ± 0.43 | 1.55 ± 0.62 | 1.68 ± 1.78 | 1.92 ± 0.92 |
| Above DCM | 3.33 ± 1.73 | 5.29 ± 3.97 | 5.48 ± 8.37 | 1.24 ± 0.78 | 1.79 ± 1.18 | 3.11 ± 5.64 | 6.24 ± 7.43 |
| DCM | 6.00 ± 4.64 | 11.64 ± 9.80 | 6.72 ± 4.71 | 1.36 ± 1.13 | 2.32 ± 1.47 | 1.73 ± 2.49 | 10.47 ± 10.01 |
| All | 3.54 ± 3.24 | 6.22 ± 6.84 | 5.04 ± 6.08 | 1.22 ± 0.82 | 1.89 ± 1.16 | 2.18 ± 3.62 | 6.21 ± 7.76 |

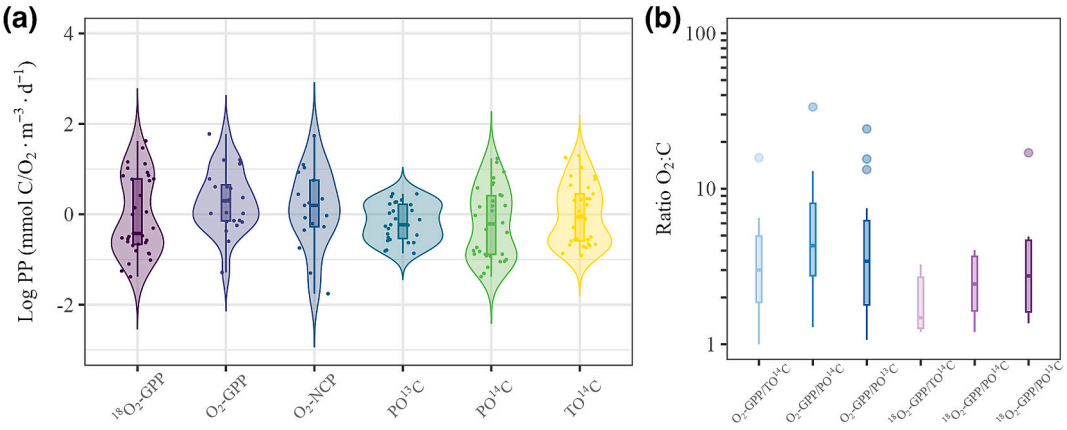


**Fig. 2.** (a) Violin plots showing volumetric primary production rates in units of mg C or $O_2 \cdot m^{-3} \cdot d^{-1}$ measured with *in situ* methods: $^{18}O_2$-GPP, $O_2$-GPP, $O_2$-NCP, $PO^{13}C$, $PO^{14}C$, and $TO^{14}C$. The shaded areas represent data density distribution, while the dots indicate actual PP rates. (b) Box plots of O:C ratios for PP estimates. In both panels, the box plots feature a rectangle representing the first and third quartiles, with the central horizontal line indicating the median. The data correspond to stations and depths where all four methods were measured.

**Table 2**
Reduced Major Axis (RMA) regressions (Model II) statistics for the relationship between log-transformed primary production rates measured using different *in situ* methods: $^{18}O_2$-GPP, $O_2$-GPP, $O_2$ NCP, $PO^{13}C$, $PO^{14}C$, and $TO^{14}C$.

| Yi | Xi | n | Intercept | Slope | $r^2$ | p-value |
|---|---|---|---|---|---|---|
| $PO^{14}C$ | $TO^{14}C$ | 33 | −0.20 | 1.15 | 0.99 | <0.01 |
| $PO^{14}C$ | $PO^{13}C$ | 27 | −0.05 | 1.69 | 0.70 | <0.01 |
| $PO^{14}C$ | $O_2$-NCP | 17 | −0.22 | 0.82 | 0.51 | <0.01 |
| $PO^{14}C$ | $O_2$-GPP | 23 | −0.66 | 1.04 | 0.67 | <0.01 |
| $PO^{14}C$ | $^{18}O_2$-GPP | 33 | −0.18 | 0.90 | 0.86 | <0.01 |
| $TO^{14}C$ | $PO^{13}C$ | 27 | 0.12 | 1.45 | 0.70 | <0.01 |
| $TO^{14}C$ | $O_2$-NCP | 17 | −0.04 | 0.73 | 0.53 | <0.01 |
| $TO^{14}C$ | $O_2$-GPP | 23 | −0.39 | 0.88 | 0.71 | <0.01 |
| $TO^{14}C$ | $^{18}O_2$-GPP | 33 | 0.02 | 0.77 | 0.87 | <0.01 |
| $TO^{13}C$ | $O_2$-NCP | 15 | −0.10 | 0.69 | 0.14 | 0.08 |
| $TO^{13}C$ | $O_2$-GPP | 21 | −0.37 | 0.73 | 0.43 | <0.01 |
| $TO^{13}C$ | $^{18}O_2$-GPP | 27 | −0.06 | 0.54 | 0.59 | <0.01 |
| $O_2$-NCP | $O_2$-GPP | 17 | −0.59 | 1.41 | 0.85 | <0.01 |
| $O_2$-NCP | $^{18}O_2$-GPP | 17 | 0.20 | 0.99 | 0.51 | <0.01 |
| $O_2$-GPP | $^{18}O_2$-GPP | 23 | 0.49 | 0.83 | 0.62 | <0.01 |

techniques ranged between 0.51 and 0.99, with *p*-values well below the significance level ($\alpha = 0.05$; Table 2). The highest $r^2$ values were observed between $^{14}C$-based and $^{18}O_2$-based estimates ($r^2 = 0.87$) (Table 2). Similar results were found between $^{14}C$-based and $O_2$-based estimates, though the correlation coefficients were lower ($0.51 < r^2 < 0.71$). In all cases, $O_2$-based method provided higher rates than C-based methods, with regressing slopes less than 1 (Table.2; Fig.S1). In contrast to $^{14}C$ estimates, $PO^{13}C$ showed poor correlation with $O_2$-based estimates ($r^2 < 0.43$), but demonstrated good agreement with $^{14}C$ and $^{18}O_2$ methods ($r^2 > 0.59$).

### 3.2. Models' performance

Integrated *in situ* PP ranged from as low as 68.30 mg $C{\cdot}m^{-2}{\cdot}d^{-1}$ at the oceanic stations to as high as 5323.66 mg $C{\cdot}m^{-2}{\cdot}d^{-1}$ at coastal stations affected by upwelling with an average value of 837.55 ± 1007.36 (Fig. 3 and Table S2). Satellite-derived NPP values fell within the range of *in situ* data, from 30.97 mg $C{\cdot}m^{-2}{\cdot}d^{-1}$ to 4924.99 mg $C{\cdot}m^{-2}{\cdot}d^{-1}$, with an average of 990.93 ± 900.23 mg $C{\cdot}m^{-2}{\cdot}d^{-1}$ (Fig. 3 and Table S3). VIIRS-based NPP generally showed lower rates than those obtained with MODIS (Fig. 3 and Table S3). Nevertheless, no statistically significant differences were identified using the Kruskal-Wallis test (*p*-value = 0.09; H = 19.08, $H_c = 21.03$).

Taylor diagrams provide a graphical summary of how closely a model's output matches observations, offering insights into the model's performance. The similarity between satellite and *in situ* data is assessed based on their correlation, the RMSD, and the amplitude of their variations, represented by their standard deviation. In these Taylor diagrams (Fig. 4), the closer a model is to the black circle representing the *in situ* data, the better its performance.

We observed a clear pattern between the performance of Chl*a*-based PP models, such as VGPM and Eppley, compared to $C_{phyto}$-based models (CbPM and CAFE) (Table 3 and Fig. 4). Excluding comparisons with $PO^{13}C$, Chl*a*-based models exhibited the highest statistically significant correlation coefficients with *in situ* techniques ($0.59 < r^2 < 0.85$), and the lowest RMSD (0.29–0.53) (Table 3 and Fig. S2). On the other hand, the VIIRS based model is the only one among the carbon-based models presenting good performance and being comparable in most cases to Chla-based models. In contrast, CAFE and MODIS-fed CbPM models showed no significant correlations, with RMSD values up to two times higher than those of Chl*a*-based models (0.52–0.73).

No significant differences were observed between Chl*a*-based models when using VIIRS or MODIS products as input data; however, VIIRS consistently yielded higher $r^2$ values and lower RMSD and bias, with very few exceptions (Table 3 and Fig. S2). Regarding CAFE, it showed poor performance in both cases. When compared with $^{14}C$, which is typically used as the 'gold standard', VGPM performed the best (Table 3 and Fig. 4a and b). Although it did not show the highest correlation coefficient ($r^2 = 0.57$–$0.83$), it accurately predicted *in situ* data (Fig. 4a and b), presenting the lowest RMSD (0.24–0.50); followed by Eppley, which had $r^2$ between 0.56 and 0.85 and RMSD of 0.44–0.64; and lastly by VIIRS-fueled CbPM ($r^2 = 0.47$–$0.80$ and RMSD = 0.29–0.54; Table 3 and Fig. S2).

The poor correlation between $C_{phyto}$-based models and *in situ* data was attributed to the underestimation of high NPP values observed in the CanEBUS and the overestimation of low NPP values at oligotrophic stations (Figs. S2, 3, 4, and 6). In contrast, Chl*a*-based models slightly overestimated low NPP values while they accurately predicting high NPP values (Figs. S2, 3, 4, and 6).

Considering each *in situ* technique separately, we observed that model performance varied among the methods (Fig. 4). As expected, since $^{14}C$ (mainly $PO^{14}C$) has historically been used as the 'gold standard' for model validation, comparisons with $TO^{14}C$ and $PO^{14}C$ displayed good performance (Fig. 4a and b). Furthermore, minor differences were observed depending on whether total or particulate $^{14}C$ uptake was used. In both cases, $VGPM_{VIIRS\&MODIS}$, and $Eppley_{VIIRS}$ were the closest models to the *in situ* data, followed by $CbPM_{VIIRS}$ and $Eppley_{MODIS}$ (Fig. 4). When $O_2$-GPP was used as the standard, VGPM and Eppley showed the best performance followed by $CbPM_{VIIRS}$ (Fig. 4d).

One of the key results was observed when $^{18}O_2$-GPP was used as the

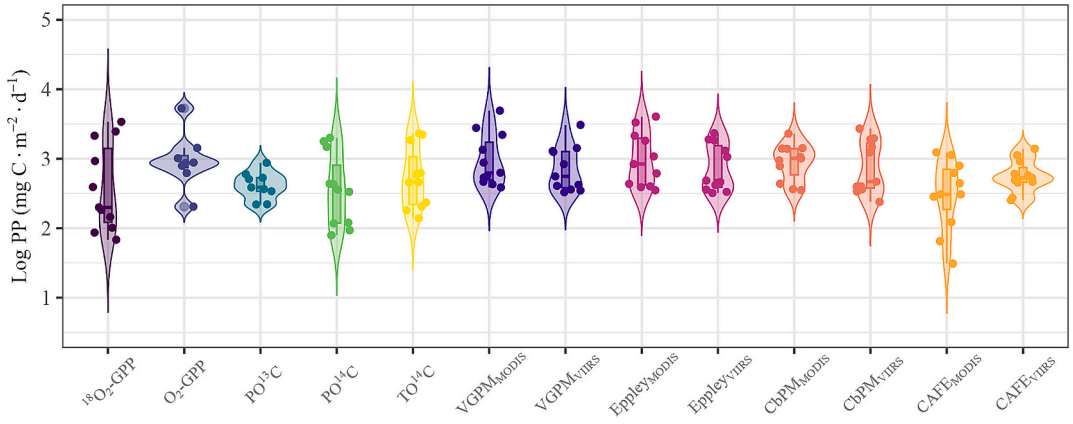


**Fig. 3.** Violin plots for integrated primary production rates (mg $C{\cdot}m^{-2}{\cdot}d^{-1}$) measured using *in situ* methods: $^{18}O_2$-GPP, $O_2$-GPP, $PO^{13}C$, $PO^{14}C$, and $TO^{14}C$.; and satellite-derived estimates (mg $C{\cdot}m^{-2}{\cdot}d^{-1}$) from models VGPM, Eppley, CbPM, and CAFE. Subscripts indicate the satellite source, either MODIS or VIIRS. Shaded areas represent data density curves, with a box plot inside each density distribution. The rectangle in the box plot shows the first and third quartiles, and the central horizontal line represents the median. Dots indicate actual PP rates.

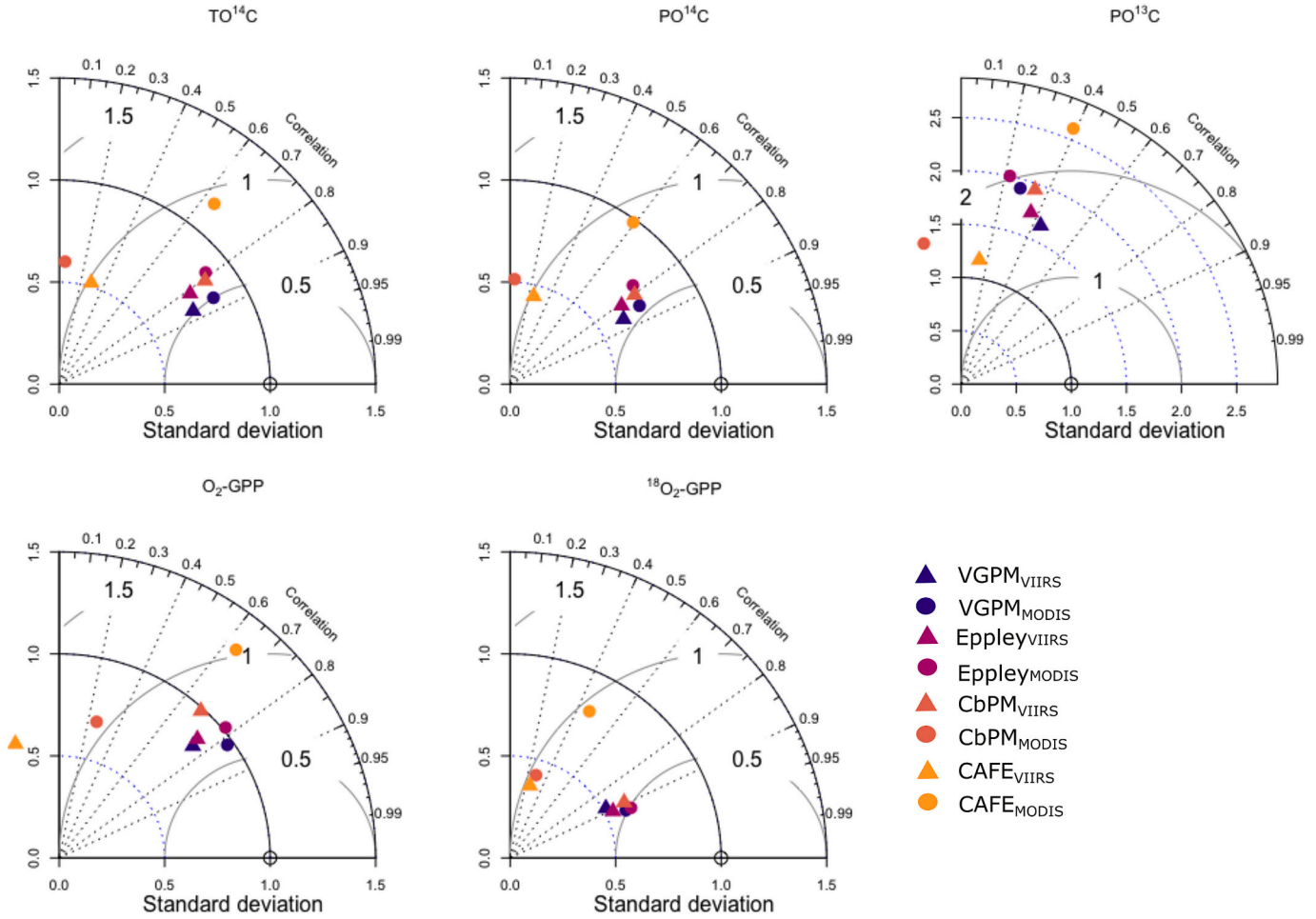


**Fig. 4.** Taylor diagrams of PP from each participating model (VGPM, Eppley, CbPM, and CAFE) and for each *in situ* technique: (a) $TO^{14}C$, (b) $PO^{14}C$, (c) $PO^{13}C$, (d) $O_2$-GPP, and (e) $^{18}O_2$-GPP. The subscript indicates the satellite source (MODIS or VIIRS). The distance from the origin (blue dotted lines) represents the standard deviation associated with the models, while the azimuth angle indicates the correlation coefficient between *in situ* and satellite PP. Black solid lines are isolines of RMSD. (For interpretation of the references to colour in this figure legend, the reader is referred to the web version of this article.)

standard. Although $^{14}C$ is the gold standard method for modeled-PP validation, we obtained better correlation using $^{18}O_2$-GPP as a benchmark, although the RMSD and bias were higher (Fig. 4e and Table 2). There were no statistically significant correlations between $PO^{13}C$ and the satellite models (Fig. 4 and Table 2).

### 3.3. Validating input data

Chl*a* and $C_{phyto}$ are key input variables for PP models. Both parameters can be derived from ocean colour data using algorithms, making their accurate retrieval critical for estimating PP. Surface Chl*a* obtained from *in situ* samples ranged from 0.07 to 2.04 mg Chl*a*·m$^{-3}$. MODIS and VIIRS closely resemble *in situ* Chl*a* estimates, spanning from 0.09 to 5.95 mg Chl*a*·m$^{-3}$ and from 0.08 to 2.59 mg Chl*a*·m$^{-3}$, respectively (Fig. 5a). Both products, MODIS and VIIRS, were well correlated with *in situ* data, with correlation coefficients of 0.73 and 0.77 and slopes of 1.06 and 0.90, respectively (Table S4). Nevertheless, VIIRS predicted *in situ* values more accurately, as indicated by its lower RMSD and bias (Fig. 5c and Table S4).

In contrast to Chl*a*, remote sensing products did not present accurate estimations of *in situ* $C_{phyto}$. The MODIS product varied between 0.52 and 41.53 mg C·m$^{-3}$, while the VIIRS product ranged from 20.02 and 66.97 mg C·m$^{-3}$, compared to *in situ* values that ranged from 8.66 and 177.52 mg C·m$^{-3}$. Although both products fall within the range of *in situ* data, they presented a significant reduced range (Fig. 5b), particularly at the higher end. This lack of accuracy was also evident in the linear correlations. Only VIIRS-based $C_{phyto}$ showed a good correlation with *in situ* data ($r^2 = 0.82$), yet the power slope was far from 1 (0.34) (Fig. 5d and Table S4). In contrast, MODIS products were poorly correlated with *in situ* data ($r^2 = 0.33$) (Fig. 5d and Table S4).

The transformation of phytoplankton biomass standing stocks, such as Chl*a* and $C_{phyto}$, into PP rates requires a biomass-normalized photosynthetic parameter, such as $P^b_{opt}$ in the case of Chl*a*-based PP models, and μ in phytoplankton biomass-based models. These parameters are theoretically computed using model-specific algorithms. In our study, satellite-derived $P^b_{opt}$ exhibited a much narrower range than *in situ* measurements. Satellite-derived $P^b_{opt}$ ranged from 4.40 to 6.83 mg C·mg Chl*a*$^{-1}$·h$^{-1}$, while *in situ* $P^b_{opt}$ ranged from 2.01 to 9.75 mg C·mg Chl*a*$^{-1}$·h$^{-1}$ (Fig. 6a). The constrained range of satellite $P^b_{opt}$ values precluded a linear correlation with *in situ* data ($r^2 < 0.07$; Fig. 6c and Table S4). A similar lack of correlation was observed between *in situ* and MODIS-derived μ ($r^2 = 0.03$). Conversely, VIIRS-derived μ showed a good correlation with *in situ* data, yet its accuracy remained low (Fig. 6d and Table S4). In this case, satellite-derived μ presented a larger range (0.20–2.00 d$^{-1}$) than *in situ* data (0.15–0.92 d$^{-1}$) (Fig. 6b). It should be noted that CbPM defines the maximum value of μ as 2, thus no higher values can be obtained.

**Table 3**
Reduced Major Axis (RMA) regressions (Model II) parameters (Intercept, Slope, $r^2$, and p-value), and performance indices (RMSD, Bias, and uRMSD) for the comparison between log-transformed *in situ* and satellite-modeled PP.

| Xi | Yi | n | Intercept | Slope | $r^2$ | p-value | RMSD | Bias | uRMSD |
|---|---|---|---|---|---|---|---|---|---|
| $TO^{14}C$ | $VGPM_{MODIS}$ | 11 | 0.69 | 0.84 | 0.75 | <0.01 | 0.33 | −0.25 | 0.21 |
| | $Eppley_{MODIS}$ | 11 | 0.57 | 0.89 | 0.62 | <0.01 | 0.37 | −0.26 | 0.26 |
| | $CbPM_{MODIS}$ | 11 | 2.56 | 0.14 | 0.01 | 0.44 | 0.53 | −0.23 | 0.48 |
| | $CAFE_{MODIS}$ | 11 | −0.43 | 1.07 | 0.41 | 0.02 | 0.48 | 0.24 | 0.39 |
| | $VGPM_{VIIRS}$ | 11 | 0.89 | 0.72 | 0.76 | <0.01 | 0.25 | −0.13 | 0.22 |
| | $Eppley_{VIIRS}$ | 11 | 0.76 | 0.78 | 0.66 | <0.01 | 0.29 | −0.15 | 0.25 |
| | $CbPM_{VIIRS}$ | 11 | 0.54 | 0.86 | 0.65 | <0.01 | 0.29 | −0.15 | 0.25 |
| | $CAFE_{VIIRS}$ | 11 | 1.76 | 0.36 | 0.09 | 0.19 | 0.42 | −0.03 | 0.42 |
| $PO^{14}C$ | $VGPM_{MODIS}$ | 11 | 1.16 | 0.71 | 0.72 | <0.01 | 0.50 | −0.42 | 0.27 |
| | $Eppley_{MODIS}$ | 11 | 1.05 | 0.76 | 0.59 | <0.01 | 0.53 | −0.43 | 0.32 |
| | $CbPM_{MODIS}$ | 11 | 2.70 | 0.09 | 0.01 | 0.45 | 0.67 | −0.39 | 0.55 |
| | $CAFE_{MODIS}$ | 11 | 0.21 | 0.89 | 0.35 | 0.03 | 0.45 | 0.07 | 0.44 |
| | $VGPM_{VIIRS}$ | 11 | 1.28 | 0.62 | 0.74 | <0.01 | 0.41 | −0.30 | 0.28 |
| | $Eppley_{VIIRS}$ | 11 | 1.18 | 0.66 | 0.65 | <0.01 | 0.44 | −0.32 | 0.30 |
| | $CbPM_{VIIRS}$ | 11 | 1.01 | 0.73 | 0.65 | <0.01 | 0.44 | −0.32 | 0.30 |
| | $CAFE_{VIIRS}$ | 11 | 2.04 | 0.28 | 0.06 | 0.22 | 0.53 | −0.20 | 0.49 |
| $PO^{13}C$ | $VGPM_{MODIS}$ | 9 | −3.16 | 2.33 | 0.08 | 0.23 | 0.47 | −0.30 | 0.36 |
| | $Eppley_{MODIS}$ | 9 | −5.49 | 3.22 | 0.05 | 0.28 | 0.49 | −0.30 | 0.38 |
| | $CbPM_{MODIS}$ | 9 | 8.14 | −2.01 | 0.06 | 0.26 | 0.42 | −0.27 | 0.32 |
| | $CAFE_{MODIS}$ | 9 | −4.08 | 2.50 | 0.15 | 0.15 | 0.47 | 0.15 | 0.44 |
| | $VGPM_{VIIRS}$ | 9 | −1.68 | 1.71 | 0.19 | 0.12 | 0.33 | −0.18 | 0.28 |
| | $Eppley_{VIIRS}$ | 9 | −2.94 | 2.20 | 0.13 | 0.17 | 0.36 | −0.19 | 0.30 |
| | $CbPM_{VIIRS}$ | 9 | −2.99 | 2.21 | 0.12 | 0.18 | 0.38 | −0.18 | 0.34 |
| | $CAFE_{VIIRS}$ | 9 | 1.31 | 0.53 | 0.02 | 0.36 | 0.25 | −0.07 | 0.24 |
| $O_2$-GPP | $VGPM_{MODIS}$ | 8 | 0.52 | 0.79 | 0.67 | <0.01 | 0.24 | 0.11 | 0.21 |
| | $Eppley_{MODIS}$ | 8 | −0.10 | 0.99 | 0.60 | 0.01 | 0.26 | 0.10 | 0.24 |
| | $CbPM_{MODIS}$ | 8 | −0.87 | 1.28 | 0.07 | 0.27 | 0.38 | 0.03 | 0.38 |
| | $CAFE_{MODIS}$ | 8 | −1.93 | 1.44 | 0.40 | 0.05 | 0.73 | 0.64 | 0.37 |
| | $VGPM_{VIIRS}$ | 8 | 0.65 | 0.71 | 0.57 | 0.02 | 0.32 | 0.21 | 0.25 |
| | $Eppley_{VIIRS}$ | 8 | −0.06 | 0.96 | 0.56 | 0.02 | 0.30 | 0.17 | 0.25 |
| | $CbPM_{VIIRS}$ | 8 | −0.40 | 1.07 | 0.47 | 0.03 | 0.33 | 0.17 | 0.28 |
| | $CAFE_{VIIRS}$ | 8 | 4.54 | 0.63 | 0.12 | 0.20 | 0.55 | 0.30 | 0.46 |
| GPP-$^{18}O_2$ | $VGPM_{MODIS}$ | 11 | 1.45 | 0.59 | 0.85 | <0.01 | 0.50 | −0.41 | 0.30 |
| | $Eppley_{MODIS}$ | 11 | 1.38 | 0.62 | 0.85 | <0.01 | 0.51 | −0.41 | 0.29 |
| | $CbPM_{MODIS}$ | 11 | 2.13 | 0.32 | 0.08 | 0.20 | 0.69 | −0.38 | 0.58 |
| | $CAFE_{MODIS}$ | 11 | 0.72 | 0.68 | 0.21 | 0.08 | 0.58 | 0.09 | 0.57 |
| | $VGPM_{VIIRS}$ | 11 | 1.55 | 0.51 | 0.78 | <0.01 | 0.45 | −0.28 | 0.36 |
| | $Eppley_{VIIRS}$ | 11 | 1.48 | 0.54 | 0.82 | <0.01 | 0.45 | −0.30 | 0.34 |
| | $CbPM_{VIIRS}$ | 11 | 1.32 | 0.60 | 0.80 | <0.01 | 0.44 | −0.30 | 0.32 |
| | $CAFE_{VIIRS}$ | 11 | 2.16 | 0.23 | 0.06 | 0.23 | 0.61 | −0.18 | 0.58 |

### 3.4. Testing models: In situ measurements as source data

To assess whether the source data affects models' performance, all models were run using *in situ* Chl*a* ($C_{phyto}$), and $P^b_{opt}$ (μ) as input data, and their performances were compared with those of satellite-fueled models. In all cases, the performance of the models improved when *in situ* data were used as inputs (Fig. 7 and Table 4). The coefficients of correlations for VGPM showed minimal change (±1 %), but the RMSD decreased by up to 43 %, the bias was reduced by 61–72 % (Table 4). In contrast, Eppley improved its coefficient of correlation by up to 24 %. The reductions in RMSD and bias were, however, comparable to those of VGPM. The most significant change occurred for CbPM, which transitioned from being uncorrelated when using MODIS data to achieving an $r^2$ of 0.74, representing an increase of three orders of magnitude when comparing with MODIS and 14 % improvement with VIIRS. Furthermore, RMSD was reduced by 39–60 %, and the bias decreased by 90–93 %, transforming CbPM from having no statistically significant correlation with $PO^{14}C$ in the case of MODIS to become the model with the best performance (Table 4).

## 4. Discussion

### 4.1. Reconciling in situ PP methods: A challenging endeavor

The various methods used to measure PP *in situ* yield variable estimates that are often difficult to compare. This has prompted the scientific community to seek ways to reconcile these differences by implementing interconversion equations, which would not only facilitate the comparisons among methods but also enable their integration into larger databases. However, studies in which PP is measured concurrently using different techniques are limited, and many focus on regions with similar environmental conditions (Arístegui et al., 1996; Arístegui and Harrison, 2002; Bender et al., 1987; Grande et al., 1989b; Grande et al., 1989a; Robinson et al., 2009; Sanz-Martín et al., 2019). The work by Regaudie-de-Gioux et al. (2014) may be an exception, as it compiles published PP data measured concurrently by at least two methods, covering the eastern North Atlantic Ocean, the western South Atlantic Ocean, and a few stations in the Indian, Antarctic, and central Pacific Oceans. Although they compare up to five different techniques, the majority of the data pertained to $^{14}C$-$^{18}O_2$ comparisons (accounting for 53 % of the individual estimates), and most PP estimations were conducted in oligotrophic regions.

The limited number of studies comparing *in situ* PP techniques have reported significant differences among methods (Bender et al., 1987; Regaudie-de-Gioux et al., 2014; Robinson et al., 2009; Sanz-Martín et al., 2019). Generally, oxygen-based methods yield higher PP rates compared to carbon-based approaches. The highest rates are typically obtained with $^{18}O_2$-GPP, followed by $O_2$-GPP, $PO^{13}C$, $TO^{14}C$, and $PO^{14}C$. While C-based methods provide estimates closer to NPP, $O_2$-based methods give estimates more representative of GPP. The $^{18}O_2$-GPP method measures total oxygen production related photosynthesis, with minimal labelled oxygen recycled through respiration during incubation (Bender et al., 1987; Cullen, 2001). The $O_2$-GPP method also captures

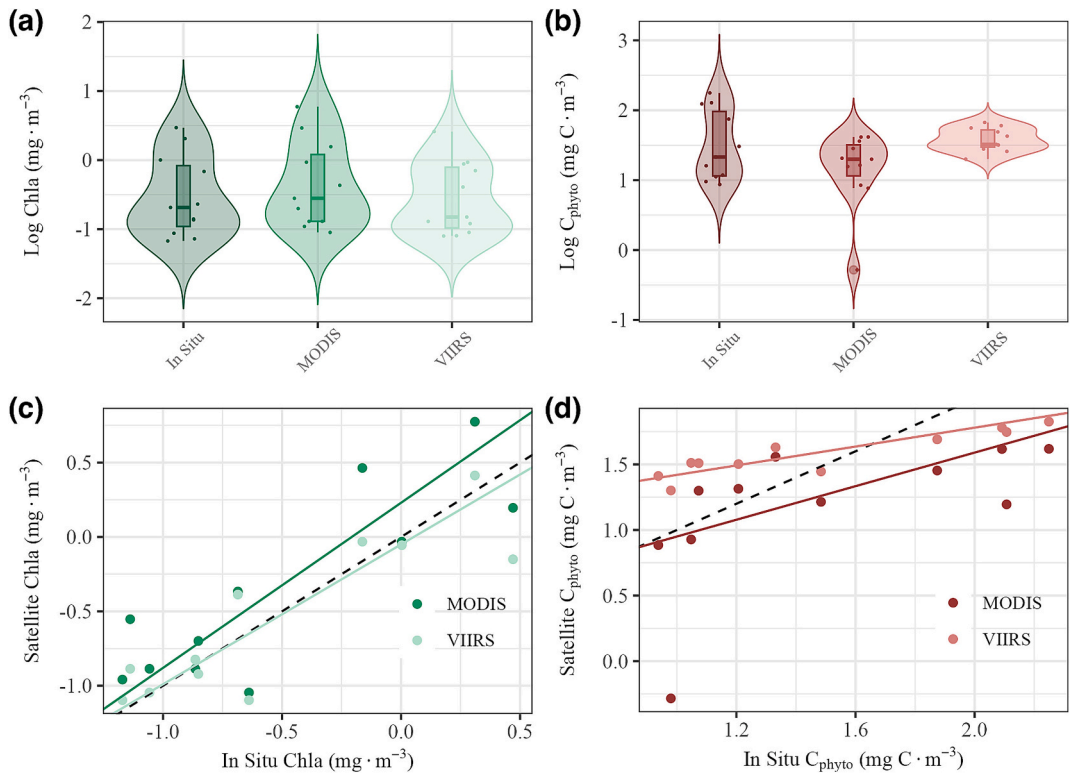


**Fig. 5.** Violin plots for (a) surface chlorophyll *a* (Chl*a*, mg Chl*a*·m$^{-3}$) measured *in situ* and derived from MODIS, and VIIRS satellites, and for (b) phytoplankton biomass ($C_{phyto}$, mg C·m$^{-3}$) measured *in situ* and derived from MODIS and VIIRS satellites. Linear regression between log-transformed (c) *in situ* and satellite derived Chl*a*, and (d) between *in situ* and satellite derived $C_{phyto}$. The black dashed line corresponds to the 1:1 regression line.

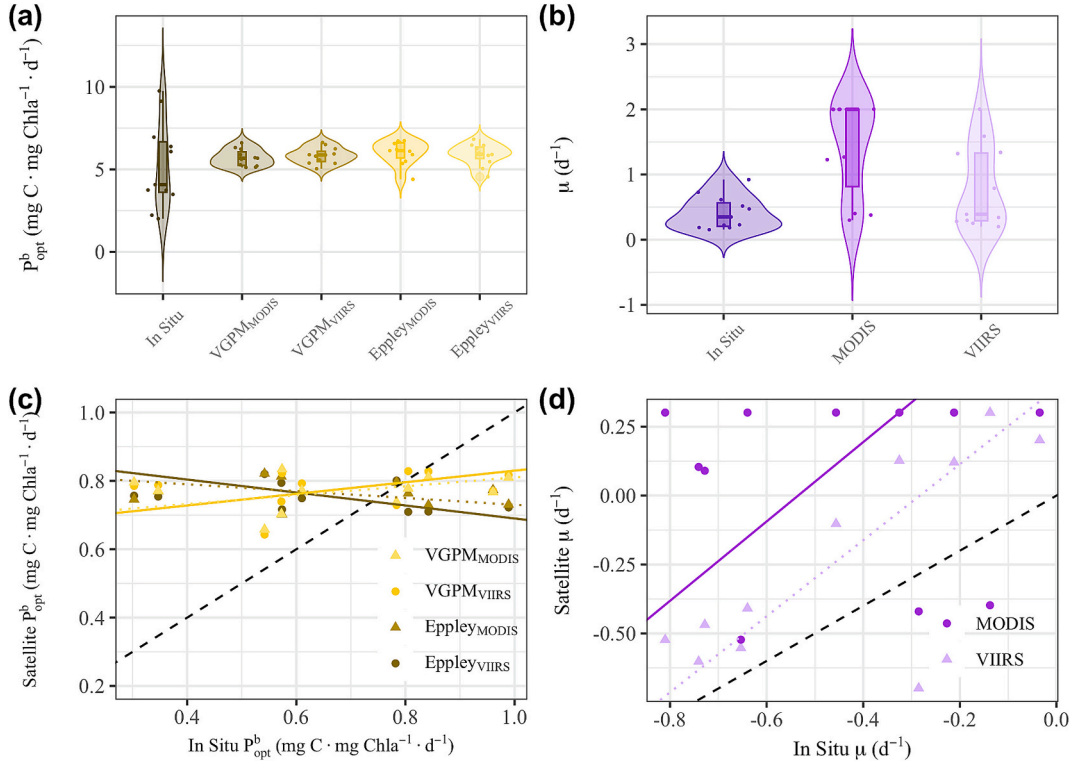


**Fig. 6.** Violin plots for (a) assimilation numbers ($P^b_{opt}$, mg C· mg Chla$^{-1}$·d$^{-1}$) calculated from *in situ* data and derived from the VGPM and Eppley models, and for (b) *in situ* growth rates (μ, d$^{-1}$) and derived from CbPM. Linear regression between log-transformed (c) *in situ* and satellite derived $P^b_{opt}$, and (d) between *in situ* and satellite derived μ. The black dashed line corresponds to the 1:1 regression line. The subscript indicates the satellite source, MODIS or VIIRS. The dotted line corresponds to VIIRS regressions.

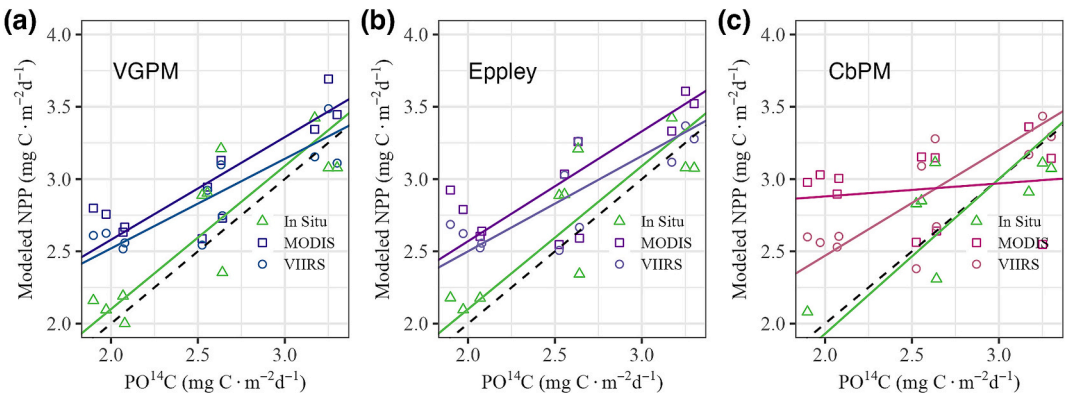


**Fig. 7.** Linear regression between log-transformed *in situ* particulate organic carbon production ($PO^{14}C$, mg C·m$^{-2}$·d$^{-1}$) and derived NPP (mg C·m$^{-2}$·d$^{-1}$) using (a) VGPM, (b) Eppley, and (c) CbPM algorithms, with *in situ* measurements and MODIS and VIIRS products as input data. The black dashed line corresponds to the 1:1 regression line.

**Table 4**
Parameters of linear regressions (Intercept, Slope, $r^2$, and p-value), along with performance indices (RMSD, and Bias), for the comparison between log-transformed *in situ* particulate organic carbon production ($PO^{14}C$) and satellite-modeled PP using *in situ* data as inputs. The values in parentheses indicate the percentage change relative to the values in Table 2, with the first value corresponding to the comparison with MODIS and the second with VIIRS.

| Xi | Yi | n | Intercept | Slope | $r^2$ (%) | p-value | RMSD (%) | Bias (%) |
|---|---|---|---|---|---|---|---|---|
| $PO^{14}C$ | $VGPM_{in\ situ}$ | 11 | 0.12 | 0.99 | 0.73 (±1) | <0.01 | 0.29 (−29/43) | −0.12 (−61/72) |
| | $Eppley_{in\ situ}$ | 11 | 0.12 | 0.99 | 0.73 (+12/24) | <0.01 | 0.29 (−34/46) | −0.11 (−64/73) |
| | $CbPM_{in\ situ}$ | 11 | −0.21 | 1.07 | 0.74 (+/14) | <0.01 | 0.27 (−39/60) | 0.03 (−90/93) |

total oxygen produced during photosynthesis but assumes that dark and light respirations are equal (Carpenter, 1965; Cullen, 2001). Both $PO^{13}C$ and $PO^{14}C$ methods yield metrics closer to NPP, as PP is measured by the amount of labelled carbon incorporated into phytoplankton biomass (Steeman-Nielsen, 1952). Differences between $O_2$-based and POC production methods are often amplified during 24-h incubations, as some of the labelled carbon incorporated into phytoplankton biomass may be respired or excreted as DOC (Marra, 2009; Milligan et al., 2015). These differences are less pronounced in the case of TOC production, which accounts for DOC excretion and therefore provides a metric closer to GPP (González et al., 2008).

Our results align with these previous studies. We found that $O_2$-based estimates were up to 60 % higher than C-based estimates (Table 1 and Fig. S1). This degree of difference between methods is consistent with other reported comparisons (Juranek and Quay, 2013; Regaudie-de-Gioux et al., 2014; Sanz-Martín et al., 2019), which observed PP rates measured using $O_2$-based techniques to be 1.5–2.5 times higher than those obtained with $^{14/13}C$ methods. Furthermore, these differences increased with depth (Table 1), suggesting an expansion of the gap between GPP and NPP. We noted the same depth-depended pattern in $DO^{14}C$ release, which showed peak rates at the DCM across all stations (Hernández-Hernández et al., 2018). Former studies have also documented increased DOC production by phytoplankton linked to light limitation in deeper ocean layers (Marañón et al., 2004; Morán and Estrada, 2001). This would reduce the amount of labelled carbon incorporated into phytoplankton biomass, potentially explaining the observed pattern. However, the moderate increase in the $O_2$-GPP:$TO^{14}C$ ratio with depth, along with relatively stable levels of $^{18}O_2$-GPP:C, suggests that these factors alone do not fully account for the observed differences (see below). Despite the significant variability in $O_2$:C ratios, our results were consistent with previously reported data in different ocean regions (Arístegui et al., 1996; Gazeau et al., 2007; Juranek and Quay, 2013; Sanz-Martín et al., 2019).

At the sea surface, $O_2$-GPP rates were up to 2-fold higher than $^{18}O_2$-GPP estimates, aligning with previous findings (Regaudie-de-Gioux et al., 2014; Robinson et al., 2009; Sanz-Martín et al., 2019). This ratio increases with depth, reaching up to 10 at the DCM. The discrepancy observed between $^{18}O_2$-GPP and $O_2$-GPP rates suggests that light respiration in our samples was lower than dark respiration, leading to an overestimation of $O_2$-GPP. Additionally, this implies that the reduction in light respiration correlated with decreased light availability, *i.e.*, increasing depth. Sanz-Martín et al. (2019) noted a similar reversal between these techniques during a low productivity season in the Arctic Ocean, dominated by small cyanobacteria-like *Synechococcus spp.* Although our study covers both high- and low-productivity regions of the CanEBUS, only 3 out of 11 stations were in eutrophic waters, while the rest corresponded to meso- and oligotrophic waters dominated by *Prochlorococcus spp* and *Synechococcus spp.*

Gazeau et al. (2007) also reported discrepancies similar to those found in our study under low light conditions. Potential explanations for these results may include the inhibition of the photorespiration, the Mehler reaction, or both, which are the primary contributors to light-dependent $O_2$ uptake by phytoplankton (Halsey and Jones, 2015), along with an increase in dark respiration during the incubation. Light respiration-related metabolic pathways are expected to be stimulated under high light intensities as dissipators of excess energy, increasing $^{18}O_2$ concentrations by approximately 20 % (Beardall et al., 2009; Laws et al., 2000). Therefore, low light availability at and above the DCM may inhibit light respiration.

On the other hand, several authors have reported an increase in dark respiration during $O_2$ evolution measurements in incubation, which in our case could be supported by higher DOC release at greater depths (Norrman et al., 1995; Puddu et al., 2003). The combined effect of these processes would lead to higher $O_2$-GPP rates compared to $^{18}O_2$-GPP. Furthermore, this hypothesis would also explain the steeper increase in $O_2$:C ratios, which are influenced by both light and dark respirations, in contrast to $^{18}O_2$:C, which only accounts for light respiration.

In contrast to our findings, previous comparisons between $PO^{13}C$ and the $PO^{14}C$ methods reported lower $PO^{14}C$ rates (López-Sandoval et al., 2018; Mousseau et al., 1995). In our study, $PO^{14}C$ rates were approximately 50 % higher than $PO^{13}C$ estimates, regardless of the productivity, despite the lower precision of the $^{13}C$ technique. It should be noted that at the most oligotrophic stations, the PP was below the detection limit of the $^{13}C$ technique in certain instances The findings of Arístegui and

Harrison (2002) are consistent with our observations. They also reported higher $PO^{14}C$ than $PO^{13}C$ rates in the northern region of the CanEBUS. Notably, there was a surprising lack of correlation between $^{13}C$ and the $O_2$-based methodologies, particularly given that the correlation coefficients among $^{14}C$, $O_2$, and $^{18}O_2$ were above 0.50. Unfortunately, with the current data, we are unable to provide a comprehensive explanation for these differences, highlighting the need for further comparative studies.

The study by Regaudie-de-Gioux et al. (2014) provides, to date, the largest available database for transforming data across *in situ* PP methods. A comparative analysis revealed that our correlation coefficients were consistently higher than those reported by Regaudie-de-Gioux et al. (Table 5). Moreover, our slopes and intercepts were closer to the ideal values of 1 and 0, respectively. The difference in slopes between the two studies ranged from 22 % to 44 %, excluding $PO^{13}C$.

The stronger correlations observed in our study may be partially attributed to the uniformity of incubation conditions across methods. Unlike Regaudie-de-Gioux et al. (2014), who compared PP rates obtained using varying incubation methodologies, we conducted all incubations under identical conditions (*i.e.*, in the same incubators and over the same time period). As discussed earlier, discrepancies in rates among different methods can be exacerbated by variations in incubation time, light, volume, and temperature.

However, it is important to note the substantial difference in database size between the two studies. The smallest dataset in Regaudie-de-Gioux et al. (2014) contains approximately four times as much data as our study, with some comparisons exceeding an order of magnitude difference in sample size, depending on the methods being analyzed.

### 4.2. Assessing model performance of NPP

From the four models tested in this study, we observed clear performance differences between Chl*a*-based and $C_{phyto}$-based models. Excluding the comparison with $PO^{13}C$, Chl*a*-based models exhibited an average $r^2$ of 0.70 ± 0.10 and RMSD of 0.38 ± 0.10 while $C_{phyto}$-based models displayed average $r^2$ values of 0.28 ± 0.26 and RMSD of 0.51 ± 0.13. Among the Chl*a*-based models, VGPM performed the best, despite being the earliest described model among those used in this work. This finding aligns with Campbell et al. (2002), who concluded that a model's predictive skill is not necessarily linked to its complexity. Eppley presented the second-highest correlation coefficients and lower RMSD values, though no significant differences were observed compared to VGPM. Although the $C_{phyto}$ provides a more precise representation of algal standing stocks, particularly in terms of NPP, which is a measure of carbon turnover rather than Chl*a*, $C_{phyto}$-based models, such as CbPM and CAFE, demonstrated significant limitations in predictive skills. These limitations were particularly evident when MODIS products were used as input data in the case of CbPM, and across all cases for the CAFE model.

To understand the limitations of the models used to accurately estimate *in situ* PP, we investigated whether these limitations arose from the input data or the models themselves. Most models rely on a phytoplankton standing stock proxy, such as Chl*a* or $C_{phyto}$, and a biomass-normalized photosynthetic parameter, such as $P^b_{opt}$ or μ. Consequently, inaccuracies in estimating either of these parameters can lead to poor model performance.

We observed that remote sensing estimates of Chl*a* presented a higher agreement with *in situ* data (Fig. 5 and Table S4) compared to the performance of VGPM and Eppley (Table. 3). This was not the case for $P^b_{opt}$, which did not exhibit a statistically significant correlation with *in situ* data. The discrepancy between the high accuracy of Chl*a* estimates and the lower performance of models utilizing these estimates can therefore be attributed to models' limited ability to accurately estimate $P^b_{opt}$.

Several studies have similarly reported weak agreement between *in situ* and satellite-derived $P^b_{opt}$, suggesting that it cannot be reliably derived using only SST (Behrenfeld and Falkowski, 1997a; Milutinović and Bertino, 2011; Regaudie-de-Gioux et al., 2019; Siegel et al., 2001). When *in situ* Chl*a* and $P^b_{opt}$ were used as input data, $r^2$ improved by up to 24 %, RMSD decreased by up to 46 % and bias was reduced by more than 70 % (Table 4). Furthermore, the differences between NPP estimates using *in situ* Chl*a* and $P^b_{opt}$, and those using satellite-derived Chl*a* but *in situ* $P^b_{opt}$, were less than 4 %.

Regarding $C_{phyto}$-based models, both the satellite-derived standing stock ($C_{phyto}$) and the biomass-normalized photosynthetic parameter (μ) showed very low agreement with *in situ* data. Although the correlations between these two sources of $C_{phyto}$ presented relatively high $r^2$ values, *in situ* $C_{phyto}$ was generally overestimated by up to 70 % (slope = 0.34). A closer examination revealed that satellite-derived $C_{phyto}$ underestimated the highest values associated with the CanEBUS stations, while it overestimated values at low-biomass oligotrophic stations.

Several studies have already reported the low accuracy of the algorithms used to estimate *in situ* $C_{phyto}$ from satellite data (Antoine et al., 2011; Behrenfeld et al., 2013; Brewin et al., 2012; Martínez-Vicente et al., 2017). On one hand, the backscatter-based ($b_{bp}$) algorithm used for $C_{phyto}$ estimation largely overlooks non-algal particles (NAP), which may represent and important fraction of organic carbon. Since the contribution of NAP to $C_{phyto}$ varies spatially, its estimation may be either under- or overestimated depending on the region of study (Bellacicco et al., 2019; Sathyendranath et al., 2009). On the other hand, Buitenhuis et al. (2012).demonstrated that $b_{bp}$ accounts for particles larger than 1 μm in spherical diameter, thus neglecting cyanobacteria-like organisms that may contribute up to 50 % of phytoplankton biomass in oligotrophic regions.

Validating remote sensing estimates of $C_{phyto}$ is a challenging task due to the inherent complexity of measuring phytoplankton biomass *in situ*. In most cases, biomass is not directly measured but derived from proxies such as particulate organic carbon or backscatter signals (Graff et al., 2015; Halsey and Jones, 2015). Consequently, direct measurements of phytoplankton carbon, which are necessary for model validation, remain scarce.

As with $P^b_{opt}$, there was no correlation between satellite-derived and *in situ* values of μ. While *in situ* data varied between 0.15 and 0.92 $d^{-1}$, more than 50 % of the MODIS-derived values were 2 $d^{-1}$, which is the

**Table 5**
Reduced Major Axis (RMA) regressions (Model II) statistics for the relationship between log-transformed primary production rates measured using different in situ methods obtained by Regaudie-de-Gioux et al. (2014) and in this study.

| Yi | Xi | Regaudie-de-Gioux et al., 2014 | | | | This study | | | |
|---|---|---|---|---|---|---|---|---|---|
| | | Slope | Intercept | $r^2$ | n | Slope | Intercept | $r^2$ | n |
| $TO^{14}C$ | $PO^{14}C$ | 0.67 | 2.25 | 0.71 | 107 | 0.86 | 0.17 | 0.99 | 33 |
| $O_2$-GPP | $TO^{14}C$ | 0.63 | 1.50 | 0.37 | 83 | 1.15 | 0.39 | 0.79 | 23 |
| $O_2$-GPP | $PO^{14}C$ | 0.76 | 2.15 | 0.49 | 657 | 0.97 | 0.59 | 0.77 | 23 |
| $PO^{13}C$ | $PO^{14}C$ | 0.88 | 1.29 | 0.69 | 198 | 0.52 | −0.06 | 0.70 | 27 |
| $^{18}O_2$-GPP | $PO^{14}C$ | 0.88 | 3.25 | 0.72 | 332 | 1.13 | 0.22 | 0.87 | 33 |
| $^{18}O_2$-GPP | $O_2$-GPP | 0.88 | 1.56 | 0.78 | 232 | 1.21 | −0.50 | 0.74 | 23 |

maximum value allowed by the algorithm. In contrast, half of the values returned by VIIRS were slightly below 2 $d^{-1}$. The maximum value of 2 $d^{-1}$ was established based on the highest Chl*a*-based phytoplankton community growth rates obtained from an extensive compilation of iron enrichment experiments (Banse, 1991; Behrenfeld et al., 2005). In a more recent review, Laws (2013) reported that most μ values in the literature were below 1 $d^{-1}$, and he observed that in tropical and subtropical regions under light-saturated conditions, μ typically corresponds to roughly 1 $d^{-1}$. This is in agreement with the *in situ* data reported here and highlights that current methods for estimating μ *via* remote sensing are far from satisfactory. This discrepancy could be attributed to the fact that these methods are based on laboratory measurements, which poorly represent the natural growth environment (Banse, 1991; Behrenfeld et al., 2005). The marked increase in CbPM accuracy when *in situ* values were used as input data supports this hypothesis.

In summary, the VGPM and Eppley models exhibited the highest accuracy in estimating NPP, regardless of the satellite source. On the other hand, CbPM showed strong correlations only when VIIRS products were used. However, we also observed that when *in situ* measurements were used as input data, the performance of all models become similar. This, along with the fact that both Chl*a* and $C_{phyto}$ showed relatively good correlation with *in situ* data, suggests that assessing the biomass-normalized photosynthetic parameters (*i.e.*, $P^b_{opt}$ and μ) could be considered the Achilles' heel in estimating NPP from remote sensing. Indeed, these parameters were not correlated with *in situ* data.

Improving satellite-based NPP estimations seems to be closely tied to advancing our understanding of the factors driving the spatial and temporal variability of photosynthesis-related parameters.

### 4.3. Potential of the different methods for models validation

The $^{14}$C-uptake method has historically been regarded as the gold standard for validating satellite-based NPP models due to its high sensitivity and precision in measuring the photosynthetic carbon retained in phytoplankton biomass. This allows for the determination of NPP even in unproductive oceans (Campbell et al., 2002; Carr et al., 2006). However, the method has several limitations. The use of radioisotopes requires specific handling and disposal procedures, which can significantly complicate, or even prevent, certain field operations. In addition, health concern and increasingly restrictive international regulations regarding their use on research vessels pose further challenges for the continued application of this method.

In fact, the majority of available $^{14}$C-based PP estimates were produced during the 1980s and 1990s as part of the Joint Global Ocean Flux Study (JGOFS), where it was a core measurement for understanding the ocean carbon cycle (Marra et al., 2021). Since then, its use has declined and has largely been replaced by other methods that are not subject to the same constraints.

The urgent need for extensive *in situ* data sets for model validation (Banks et al., 2020; Brewin et al., 2021; Groom et al., 2019; IPCC, 2022) is thus in direct conflict with the decreasing use of the $^{14}$C technique. Therefore, for future model validations, it may be necessary to turn to alternative methods that can generate a large *in situ* dataset.

Our results highlight the potential of the $^{18}O_2$ method, which demonstrated the highest agreement with Chl*a*-based models, though it tended to overestimate them. This overestimation could be attributed to the use of a single photosynthetic quotient (PQ) for all samples to convert $O_2$ to C units. Our findings show that the C:$O_2$ ratios vary between stations and with depth, suggesting that a fixed PQ may not be appropriate across all conditions.

Another possible explanation for the overestimation is that $O_2$-based methods provide GPP estimates, whereas C-based techniques measure metrics close to either NPP or GPP, depending on the fraction of primary production considered and the incubation time (González et al., 2008; Marra, 2009; Milligan et al., 2015). However, whether GPP or NPP provides more valuable information for biogeochemical, or climate change studies require further discussion (Juranek and Quay, 2013; Palevsky et al., 2016; Westberry et al., 2023). GPP accounts for $CO_2$ fixed during photosynthesis, regardless of the subsequent fate of the organic carbon produced, while NPP measures the amount of photosynthetically fixed carbon available to the upper heterotrophic levels in the ecosystem.

From the perspective of the total atmospheric $CO_2$ captured by the ocean in biological processes, GPP may provide a more useful metric than NPP. For example, recent satellite-based biogeochemical studies have reported global GPP estimates that are ~1.5–2.2 times greater than NPP (Huang et al., 2021; Westberry and Behrenfeld, 2014). However, if the carbon cycle in the ocean is to be studied in more detail, NPP seems to provide more insight into the fate of photosynthetically transformed organic carbon and its relationship with other processes within the Biological Carbon Pump, beyond photosynthesis.

It is true that additional measurements of dissolved organic carbon (DOC) production are necessary to fully understand the relationship between primary production and the microbial loop. With the $O_2$ evolution method, both GPP and NPP, along with the community respiration, are measured. However, implementing this method is not without complexity, as it assumes equal light and dark respiration -an assumption that cannot be applied in all cases (Beardall, 1989; González et al., 2008; Grande et al., 1989a). Furthermore, as Marra and Barber (2004) pointed out, nearly all the $CO_2$ respired during the day is re-fixed during photosynthesis, which suggests that twice the dark carbon loss equals the 24-h rate of phytoplankton respiration. As observed in this study, such assumption may lead to negative NPP estimates, which could conflict with remote sensing-based estimates. In contrast, the $^{18}O_2$ method does not require this assumption, as it is only affected by light respiration.

Despite the fact that the $^{13}$C method did not correlate well with any of the tested models, its good agreement with the $^{14}$C method suggests that it could be a viable alternative for model validation. Unlike $^{14}$C, $^{13}$C is not subject to the risks associated with the use of radioactive isotopes. However, due to the lower sensitivity of the mass-spectrometry technique used for quantifying stable isotopes compared to scintillation counters, it requires larger sample volumes and incubation times longer than 1 h. As a result, it is not a suitable method for measuring photosynthetic parameters through photosynthesis-irradiance (P-I) curves. Furthermore, because this method measures the enrichment of $^{13}$C relative to $^{12}$C, the accuracy of the technique depends on knowing the initial isotopic ratio of the particulate organic carbon (POC).

Uncertainties regarding the specific component of the PP addressed by each technique present another argument in favor of the $^{18}O_2$ method. While interpreting carbon uptake measurements is often complex, and $O_2$–based techniques require certain assumptions, there is general consensus about what the $^{18}O_2$ method measures (Bender et al., 1987; Cullen, 2001). As a result, interpreting $^{18}O_2$ data is less encumbered by the ambiguities associated with other methods.

One counter-argument against all $O_2$-based methods, including $^{18}O_2$, is the need to apply the molar ratio of $O_2$ produced to $CO_2$ fixed – the photosynthetic quotient (PQ)- to convert $O_2$ measurements into PP rates expressed in carbon units. While theoretically, PQ should range from 1 (synthesis of carbohydrates) to a maximum of 1.5 (synthesis of lipids), reported values range widely from >1 to 4 (Freitas et al., 2020; Trentman et al., 2023), influenced by a variety of environmental, taxonomic, and metabolic factors. In this study $^{18}O_2$:$^{14}$C ratios ranged from 0.5 to 2.4, while $O_2$:$^{14}$C varied more widely, from 0.5 to 10, with a clear depth-dependent pattern.

## 5. Conclusions

The concurrent measurement of *in situ* PP rates using four different techniques across the highly contrasting regions presented here offers a

rare opportunity to explore the fundamental differences in the specific components of PP addressed by each method, and to develop equations that enable comparison of rates derived from these techniques. However, from our results and previous attempts to reconcile *in situ* PP methods, it is evident that differences among techniques are difficult to reconcile. Several factors lead us to this conclusion: (1) Different techniques measure distinct components of PP, and in some cases, it is not possible to distinguish them; (2) Variations in incubation procedures may lead to changes in the component of PP assessed by each technique; and (3) Environmental and biological factors may influence PP measurements obtained through different methods in diverse ways. All the above makes it difficult to establish reliable correlations between techniques. We agree with other authors who suggest using a combination of methods in any research focused in PP. At the very least, the choice of method should align with the specific question being addressed.

Regarding NPP estimate from satellites, we observed that the earliest algorithms, *i.e.*, the Chl*a*-based models, produced the most accurate NPP estimates in our region of study. Furthermore, our results indicate that VIIRS products resulted in a more accurate NPP estimates than MODIS products, despite their lower resolution. However, our findings also suggest that the primary limitation of the NPP models tested here lies in their inability to accurately estimate $P^b_{opt}$ and μ. These two essential parameters are crucial for converting phytoplankton standing stocks into PP rates, yet they have been scarcely studied in natural phytoplankton communities. We conclude that future efforts should prioritize improving our understanding of the factors driving these parameters in natural environments to enhance the reliability of model-derived $P^b_{opt}$ and μ and thereby improve NPP estimates.

## CRediT authorship contribution statement

**Nauzet Hernández-Hernández:** Writing – review & editing, Writing – original draft, Visualization, Software, Investigation, Formal analysis, Conceptualization. **Yeray Santana-Falcón:** Writing – review & editing, Visualization, Software, Formal analysis. **María F. Montero:** Writing – review & editing, Investigation. **Mar Benavides:** Writing – review & editing, Investigation. **Antonio Delgado-Huertas:** Writing – review & editing, Investigation. **Xosé A. Álvarez-Salgado:** Writing – review & editing, Investigation. **Peter Land:** Writing – review & editing, Investigation. **Javier Arístegui:** Writing – review & editing, Investigation, Funding acquisition, Formal analysis, Conceptualization.

## Funding

This work was funded by the Spanish National Plan for Scientific and Technical Research and Innovation research grant FLUXES (CTM2015-69392-C3), co-financed with FEDER funds. Additional support was provided by the projects e-IMPACT (PID2019-109084RB-C21), ESA 4DAtlantic EBUS PRIMUS (ESA Contract No. 4000135025/21/I-NB), OceanICU (HORIZON-CL6-2022-CLIMATE-01-02; 101083922), and the US National Science Foundation grant OCE-1840868 awarded to the Scientific Committee on Oceanic Research (SCOR) WG 155. NH-H was supported by a grant (TESIS2015010036) from the Agencia Canaria de Investigación, Innovación, y Sociedad de la Información (ACIISI) during the cruise and data analysis.

## Declaration of competing interest

The authors declare that they have no known competing financial interests or personal relationships that could have appeared to influence the work reported in this paper.

## Acknowledgements

We would like to express our gratitude to the Unit of Marine Technology (UTM) of the Spanish Research Council (CSIC) and the crew of the R/V Sarmiento de Gamboa for their invaluable assistance at sea. Additionally, we would like to acknowledge Søren Hallstrøm, Isabel Baños, and Arsenio Granados for their contributions to $^{13}C$, $O_2$, and $^{18}O_2$ measurements at sea, respectively, and to the Group of Biological Oceanography (GOB) for their technical support in the analysis of phytoplankton and chlorophyll *a* samples.

## Appendix A. Supplementary data

Supplementary data to this article can be found online at https://doi.org/10.1016/j.jmarsys.2025.104109.

## Data availability

Data will be made available on request.

## References

Antoine, D., Siegel, D.A., Kostadinov, T., Maritorena, S., Nelson, N.B., Gentili, B., Vellucci, V., Guillocheau, N., 2011. Variability in optical particle backscattering in contrasting bio-optical oceanic regimes. Limnol. Oceanogr. 56, 955–973. https://doi.org/10.4319/lo.2011.56.3.0955.

Arístegui, J., Harrison, W.G., 2002. Decoupling of primary production and community respiration in the ocean: implications for regional carbon studies. Aquat. Microb. Ecol. 29, 199–209.

Arístegui, J., Montero, M.F., Ballesteros, S., Basterretxea, G., Van Lenning, K., 1996. Planktonic primary production and microbial respiration measured by 14 C assimilation and dissolved oxygen changes in coastal waters of the Antarctic Peninsula during austral summer: implications for carbon flux studies. Mar. Ecol. Prog. Ser. 132, 191–201.

Arístegui, J., Barton, E.D., Álvarez-Salgado, X.A., Santos, A.M.P., Figueiras, F.G., Kifani, S., Hernández-León, S., Mason, E., Machú, E., Demarcq, H., 2009. Sub-regional ecosystem variability in the Canary Current upwelling. Prog. Oceanogr. 83, 33–48. https://doi.org/10.1016/j.pocean.2009.07.031.

Banks, A.C., Vendt, R., Alikas, K., Bialek, A., Kuusk, J., Lerebourg, C., Ruddick, K., Tilstone, G., Vabson, V., Donlon, C., Casal, T., 2020. Fiducial reference measurements for satellite ocean colour (FRM4SOC). Remote Sens. 12. https://doi.org/10.3390/RS12081322.

Banse, K., 1991. Rates of phytoplankton cell division in the field and in iron enrichment experiments. Limnol. Oceanogr. 36, 1886–1898. https://doi.org/10.4319/lo.1991.36.8.1886.

Barange, M., Merino, G., Blanchard, J., Scholtens, J., Harle, J., Allison, E.H., Allen, J.I., Holt, J., Jennings, S., 2014. Impacts of climate change on marine ecosystem production in societies dependent of fisheries. Nat. Clim. Chang. 4, 211–216. https://doi.org/10.1038/nclimate2119.

Basterretxea, G., Arístegui, J., 2000. Mesoscale variability in phytoplankton biomass distribution and photosynthetic parameters in the Canary-NW African coastal transition zone. Mar. Ecol. Prog. Ser. 197, 27–40.

Beardall, J., 1989. Photosynthesis and Photorespiration in Marine Organisms. Aquat. Bot. 34, 105–130.

Beardall, J., Ihnken, S., Quigg, A., 2009. Gross and net primary production: closing the gap between concepts and measurements. Aquat. Microb. Ecol. 113–122. https://doi.org/10.3354/ame01305.

Behrenfeld, M.J., Falkowski, P.G., 1997a. A consumer's guide to phytoplankton primary productivity models. Limnol. Oceanogr. 42, 1479–1491. https://doi.org/10.4319/lo.1997.42.7.1479.

Behrenfeld, M.J., Falkowski, P.G., 1997b. Photosynthetic rates derived from satellite-based chlorophyll concentration. Limnol. Oceanogr. 42, 1–20.

Behrenfeld, M.J., Boss, E., Siegel, D.A., Shea, D.M., 2005. Carbon-based ocean productivity and phytoplankton physiology from space. Glob. Biogeochem. Cycles 19, 1–14. https://doi.org/10.1029/2004GB002299.

Behrenfeld, M.J., Hu, Y., Hostetler, C.A., Dall'Olmo, G., Rodier, S.D., Hair, J.W., Trepte, C.R., 2013. Space-based lidar measurements of global ocean carbon stocks. Geophys. Res. Lett. 40, 4355–4360. https://doi.org/10.1002/grl.50816.

Bellacicco, M., Cornec, M., Organelli, E., Brewin, R.J.W., Neukermans, G., Volpe, G., Barbieux, M., Poteau, A., Schmechtig, C., D'Ortenzio, F., Marullo, S., Claustre, H., Pitarch, J., 2019. Global Variability of Optical Backscattering by Non-algal particles From a Biogeochemical-Argo Data Set. Geophys. Res. Lett. 46, 9767–9776. https://doi.org/10.1029/2019GL084078.

Bender, M., Grande, K., Johnson, K., Marra, J., Williams, P.J.L.B., Sieburth, J., Pilson, M., Langdon, C., Hitchcock, G., Orchardo, J., Hunt, C., Donaghay, P., Heinemann, K., 1987. A comparison of four methods for determining planktonic community production. Limnol. Oceanogr. 32, 1085–1098. https://doi.org/10.4319/lo.1987.32.5.1085.

Bender, M., Orchardo, J., Dickson, M.-L., Barber, R., Lindley, S., 1999. In vitro O2 fluxes compared with 14C production and other rate terms during the JGOFS Equatorial Pacific experiment. Deep-Sea Res. I 46, 637–654.

Bindoff, N.L., Cheung, W.W.L., Kairo, J.G., 2022. Changing Ocean, Marine Ecosystems, and Dependent Communities. In: The Ocean and Cryosphere in a Changing Climate:

Special Report of the Intergovernmental Panel on Climate Change. Cambridge University Press, pp. 447–588. https://doi.org/10.1017/9781009157964.007.
Bjørnsen, P.K., 1986. Automatic Determination of Bacterioplankton Biomass by Image Analysist. Appl. Environ. Microbiol. 51, 1199–1204.
Block, B.A., Jonsen, I.D., Jorgensen, S.J., Winship, A.J., Shaffer, S.A., Bograd, S.J., Hazen, E.L., Foley, D.G., Breed, G.A., Harrison, A.-L., Ganong, J.E., Swithenbank, A., Castleton, M., Dewar, H., Mate, B.R., Shillinger, G.L., Schaefer, K.M., Benson, S.R., Weise, M.J., Henry, R.W., Costa, D.P., 2011. Tracking apex marine predator movements in a dynamic ocean. Nature 475, 86–90. https://doi.org/10.1038/nature10082.
Blythe, J., Armitage, D., Alonso, G., Campbell, D., Esteves Dias, A.C., Epstein, G., Marschke, M., Nayak, P., 2020. Frontiers in coastal well-being and ecosystem services research: a systematic review. Ocean Coast. Manag. https://doi.org/10.1016/j.ocecoaman.2019.105028.
Børsheim, Y.K., Bratbak, G., 1987. Cell volume to cell carbon conversion factors for a bacterivorous Monas sp. enriched from seawater. Mar. Ecol. Prog. Ser. 36, 171–175.
Bouman, H.A., Platt, T., Doblin, M., Figueiras, F.G., Gudmundsson, K., Gudfinnsson, H. G., Huang, B., Hickman, A., Hiscock, M., Jackson, T., Lutz, V.A., Mélin, F., Rey, F., Pepin, P., Segura, V., Tilstone, G.H., Van Dongen-Vogels, V., Sathyendranath, S., 2018. Photosynthesis-irradiance parameters of marine phytoplankton: Synthesis of a global data set. Earth Syst. Sci. Data 10, 251–266. https://doi.org/10.5194/essd-10-251-2018.
Brewin, R.J.W., Dall'Olmo, G., Sathyendranath, S., Hardman-Mountford, N.J., 2012. Particle backscattering as a function of chlorophyll and phytoplankton size structure in the open-ocean. Opt. Express 20, 17632–17652. https://doi.org/10.1364/OE.20.017632.
Brewin, R.J.W., Sathyendranath, S., Platt, T., Bouman, H., Ciavatta, S., Dall'Olmo, G., Dingle, J., Groom, S., Jönsson, B., Kostadinov, T.S., Kulk, G., Laine, M., Martínez-Vicente, V., Psarra, S., Raitsos, D.E., Richardson, K., Rio, M.H., Rousseaux, C.S., Salisbury, J., Shutler, J.D., Walker, P., 2021. Sensing the ocean biological carbon pump from space: a review of capabilities, concepts, research gaps and future developments. Earth Sci. Rev. https://doi.org/10.1016/j.earscirev.2021.103604.
Bryan, J.R., Rlley, J.P., Williams, P.J.Leb, 1976. A winkler procedure for making precise measurements of oxygen concentration for productivity and related studies. J. Exp. Mar. Biol. Ecol. 21, 191–197. https://doi.org/10.1016/0022-0981(76)90114-3.
Buitenhuis, E.T., Li, W.K.W., Vaulot, D., Lomas, M.W., Landry, M.R., Partensky, F., Karl, D.M., Ulloa, O., Campbell, L., Jacquet, S., Lantoine, F., Chavez, F., MacIas, D., Gosselin, M., McManus, G.B., 2012. Picophytoplankton biomass distribution in the global ocean. Earth Syst. Sci. Data 4, 37–46. https://doi.org/10.5194/essd-4-37-2012.
Campbell, J.W., Antoine, D., Armstrong, R., Arrigo, K., Balch, W., Barber, R., Behrenfeld, M., Bidigare, R., Bishop, J., Carr, M.E., Esaias, W., Falkowski, P., Hoepffner, N., Iverson, R., Kiefer, D., Lohrenz, S., Marra, J., Morel, A., Ryan, J., Vedernikov, V., Waters, K., Yentsch, C., Yoder, J., 2002. Comparison of algorithms for estimating ocean primary production from surface chlorophyll, temperature, and irradiance. Glob. Biogeochem. Cycles 16. https://doi.org/10.1029/2001gb001444.
Carpenter, J.H., 1965. The accuracy of the Winkler method for dissolved oxygen analysis. Limnol. Oceanogr. 10, 135–140.
Carr, M.-E., 2002. Estimation of potential productivity in Eastern Boundary Currents using remote sensing. Deep-Sea Res. II 49, 59–80.
Carr, M.E., Friedrichs, M.A.M., Schmeltz, M., Noguchi Aita, M., Antoine, D., Arrigo, K.R., Asanuma, I., Aumont, O., Barber, R., Behrenfeld, M., Bidigare, R., Buitenhuis, E.T., Campbell, J., Ciotti, A., Dierssen, H., Dowell, M., Dunne, J., Esaias, W., Gentili, B., Gregg, W., Groom, S., Hoepffner, N., Ishizaka, J., Kameda, T., Le Quéré, C., Lohrenz, S., Marra, J., Mélin, F., Moore, K., Morel, A., Reddy, T.E., Ryan, J., Scardi, M., Smyth, T., Turpie, K., Tilstone, G., Waters, K., Yamanaka, Y., 2006. A comparison of global estimates of marine primary production from ocean color. Deep-Sea Res. II Top. Stud. Oceanogr. 53, 741–770. https://doi.org/10.1016/j.dsr2.2006.01.028.
Cullen, J.J., 2001. Primary production methods. In: Encyclopedia of Ocean Sciences. Elsevier, pp. 2277–2284. https://doi.org/10.1006/rwos.2001.0203.
Dorans, N.J., Holland, P.W., 2000. Population invariance and the equatability of tests: basic theory and the linear case. J. Educ. Meas. 37, 281–306.
Eppley, R.W., 1972. Temperature and phytoplankton growth in the sea. Fish. Bull. 70, 1063–1085.
Fahey, T., Knapp, A.K., 2007. Principles and Standards for Measuring Primary Production, 1st ed. Oxford Academic, New York. https://doi.org/10.1093/acprof:oso/9780195168662.001.0001.
FAO, 2022. The State of World Fisheries and Aquaculture 2022. FAO. https://doi.org/10.4060/cc0461en.
Freitas, H.F., White, A.E., Quay, P.D., 2020. Diel measurements of oxygen- and carbon-based ocean metabolism across a trophic gradient in the North Pacific. Glob. Biogeochem. Cycles 34. https://doi.org/10.1029/2019GB006518.
Fréon, P., Arístegui, J., Bertrand, A., Crawford, R.J.M., Field, J.C., Gibbons, M.J., Tam, J., Hutchings, L., Masski, H., Mullon, C., Ramdani, M., Seret, B., Simier, M., 2009. Functional group biodiversity in Eastern Boundary Upwelling Ecosystems questions the wasp-waist trophic structure. Prog. Oceanogr. 83, 97–106. https://doi.org/10.1016/j.pocean.2009.07.034.
Friedrichs, M.A.M., Carr, M.E., Barber, R.T., Scardi, M., Antoine, D., Armstrong, R.A., Asanuma, I., Behrenfeld, M.J., Buitenhuis, E.T., Chai, F., Christian, J.R., Ciotti, A.M., Doney, S.C., Dowell, M., Dunne, J., Gentili, B., Gregg, W., Hoepffner, N., Ishizaka, J., Kameda, T., Lima, I., Marra, J., Mélin, F., Moore, J.K., Morel, A., O'Malley, R.T., O'Reilly, J., Saba, V.S., Schmeltz, M., Smyth, T.J., Tjiputra, J., Waters, K., Westberry, T.K., Winguth, A., 2009. Assessing the uncertainties of model estimates of primary productivity in the tropical Pacific Ocean. J. Mar. Syst. 76, 113–133. https://doi.org/10.1016/j.jmarsys.2008.05.010.
García-Reyes, M., Sydeman, W.J., Schoeman, D.S., Rykaczewski, R.R., Black, B.A., Smit, A.J., Bograd, S.J., 2015. Under pressure: climate change, upwelling, and eastern boundary upwelling ecosystems. Front. Mar. Sci. https://doi.org/10.3389/fmars.2015.00109.
Gazeau, F., Middelburg, J.J., Loijens, M., Vanderborght, J.P., Pizay, M.D., Gattuso, J.P., 2007. Planktonic primary production in estuaries: comparision of 14C, O2, and 18O methods. Aquat. Microb. Ecol. 46, 95–106.
Gómez-Letona, M., Ramos, A.G., Coca, J., Arístegui, J., 2017. Trends in primary production in the canary current upwelling system-A regional perspective comparing remote sensing models. Front. Mar. Sci. 4. https://doi.org/10.3389/fmars.2017.00370.
González, N., Gattuso, J.P., Middelburg, J.J., 2008. Oxygen production and carbon fixation in oligotrophic coastal bays and the relationship with gross and net primary production. Aquat. Microb. Ecol. 52, 119–130. https://doi.org/10.3354/ame01208.
Graff, J.R., Westberry, T.K., Milligan, A.J., Brown, M.B., Dall'Olmo, G., van Dongen-Vogels, V., Reifel, K.M., Behrenfeld, M.J., 2015. Analytical phytoplankton carbon measurements spanning diverse ecosystems. Deep-Sea Res. I Oceanogr. Res. Pap. 102, 16–25. https://doi.org/10.1016/j.dsr.2015.04.006.
Grande, K.D., Marra, J., Langdon, C., Heinemann, K., Bender, M.L., 1989a. Rates of respiration in the light measured in marine phytoplankton using an 0 isotope-labelling technique. J. Exp. Mar. Biol. Ecol. 129, 95–120.
Grande, K.D., Williams, P.J.L., Marra, J., Purdie, D.A., Heinemann, K., Eppleyii, R.W., Bender, M.L., 1989b. Primary Production in the North Pacific Gyre: A Comparison of Rates Determined by the 14C, O2 Concentration and 18O Methods.
Groom, S.B., Sathyendranath, S., Ban, Y., Bernard, S., Brewin, B., Brotas, V., Brockmann, C., Chauhan, P., Choi, J.K., Chuprin, A., Ciavatta, S., Cipollini, P., Donlon, C., Franz, B.A., He, X., Hirata, T., Jackson, T., Kampel, M., Krasemann, H., Lavender, S.J., Pardo-Martinez, S., Melin, F., Platt, T., Santoleri, R., Skakala, J., Schaeffer, B., Smith, M., Steinmetz, F., Valente, A., Wang, M., 2019. Satellite ocean colour: current status and future perspective. Front. Mar. Sci. https://doi.org/10.3389/fmars.2019.00485.
Hallstrøm, S., Benavides, M., Salamon, E.R., Arístegui, J., Riemann, L., 2022. Activity and distribution of diazotrophic communities across the Cape Verde Frontal Zone in the Northeast Atlantic Ocean. Biogeochemistry 160, 49–67. https://doi.org/10.1007/s10533-022-00940-w.
Halsey, K.H., Jones, B.M., 2015. Phytoplankton strategies for photosynthetic energy allocation. Annu. Rev. Mar. Sci. 7, 265–297. https://doi.org/10.1146/annurev-marine-010814-015813.
Hama, Hama, Handa, 1993. 13C tracer methodology in microbial ecology with special reference to primary production processes in aquatic environments. In: Advances in Microbial Ecology. Springer, US, Boston, MA, pp. 39–83.
Hansen, H.P., 1999. Determination of oxygen. In: Methods of Seawater Analysis. John Wiley & Sons, Ltd, pp. 75–89. https://doi.org/10.1002/9783527613984.ch4.
Hernández-Hernández, N., Bach, L.T., Montero, M.F., Taucher, J., Baños, I., Guan, W., Espósito, M., Ludwig, A., Achterberg, E.P., Riebesell, U., Arístegui, J., 2018. High CO2 under nutrient fertilization increases primary production and biomass in subtropical phytoplankton communities: a mesocosm approach. Front. Mar. Sci. 5. https://doi.org/10.3389/fmars.2018.00213.
Holm-Hansen, O., Lorenzen, C.J., Holmes, R.W., Strickland, J.D.H., 1965. Fluorometric Determination of Chlorophyll. ICES J. Mar. Sci. 30, 3–15. https://doi.org/10.1093/icesjms/30.1.3.
Huang, Y., Nicholson, D., Huang, B., Cassar, N., 2021. Global estimates of marine gross primary production based on machine learning upscaling of field observations. Glob. Biogeochem. Cycles 35. https://doi.org/10.1029/2020GB006718.
IPCC, 2022. Changing ocean, marine ecosystems, and dependent communities. In: The Ocean and Cryosphere in a Changing Climate. Cambridge University Press, pp. 447–588. https://doi.org/10.1017/9781009157964.007.
Juranek, L.W., Quay, P.D., 2013. Using triple isotopes of dissolved oxygen to evaluate global marine productivity. Annu. Rev. Mar. Sci. 5, 503–524. https://doi.org/10.1146/annurev-marine-121211-172430.
Kämpf, J., Chapman, P., 2018. Upwelling Systems of the World: A Scientific Journey to the Most Productive Marine Ecosystems, 2nd ed. Springer Cham. https://doi.org/10.1007/978-3-319-42524-5.
Kolber, Z., Falkowski, P.G., 1993. Use of active fluorescence to estimate phytoplankton photosynthesis in situ. Limnol. Oceanogr. 38, 1646–1665. https://doi.org/10.4319/lo.1993.38.8.1646.
Kruskal, W.H., Wallis, W.A., 1952. Use of ranks in one-criterion variance analysis. J. Am. Stat. Assoc. 47, 583–621. https://doi.org/10.1080/01621459.1952.10483441.
Kulk, G., Platt, T., Dingle, J., Jackson, T., Jönsson, B.F., Bouman, H.A., Babin, M., Brewin, R.J.W., Doblin, M., Estrada, M., Figueiras, F.G., Furuya, K., González-Benítez, N., Gudfinnsson, H.G., Gudmundsson, K., Huang, B., Isada, T., Kovač, Ž., Lutz, V.A., Marañón, E., Raman, M., Richardson, K., Rozema, P.D., van de Poll, W.H., Segura, V., Tilstone, G.H., Uitz, J., van Dongen-Vogels, V., Yoshikawa, T., Sathyendranath, S., 2020. Primary production, an index of climate change in the ocean: satellite-based estimates over two decades. Remote Sens. 12. https://doi.org/10.3390/rs12050826.
Lachkar, Z., Gruber, N., 2012. A comparative study of biological production in eastern boundary upwelling systems using an artificial neural network. Biogeosciences 9, 293–308. https://doi.org/10.5194/bg-9-293-2012.
Laws, E.A., 2013. Evaluation of in situ phytoplankton growth rates: A synthesis of data from varied approaches. Annu. Rev. Mar. Sci. 5, 247–268. https://doi.org/10.1146/annurev-marine-121211-172258.
Laws, E.A., Landry, M.R., Barber, R.T., Campbell, L., Dickson, M.-L., Marra, J., Biology, M., Doherty, L., 2000. Carbon cycling in primary production bottle incubations: inferences from grazing experiments and photosynthetic studies using C and O in the Arabian Sea. Deep-Sea Res. II 47, 1339–1352.

Lee, Z., Marra, J., Perry, M.J., Kahru, M., 2015. Estimating oceanic primary productivity from ocean color remote sensing: A strategic assessment. J. Mar. Syst. 149, 50–59. https://doi.org/10.1016/j.jmarsys.2014.11.015.

Levin, L.A., Le Bris, N., 2015. The deep ocean under climate change. Science 1979 (350), 766–768. https://doi.org/10.1126/science.aad0126.

López-Sandoval, D.C., Delgado-Huertas, A., Agustí, S., 2018. The 13 C method as a robust alternative to 14 C-based measurements of primary productivity in the Mediterranean Sea. J. Plankton Res. 40, 544–554. https://doi.org/10.1093/plankt/fby031.

Lottig, N.R., Phillips, J.S., Batt, R.D., Scordo, F., Williamson, T.J., Carpenter, S.R., Chandra, S., Hanson, P.C., Solomon, C.T., Vanni, M.J., Zwart, J., 2022. Estimating pelagic primary production in lakes: comparison of 14C incubation and free-water O2 approaches. Limnol. Oceanogr. Methods 20, 34–45. https://doi.org/10.1002/lom3.10471.

Luz, B., Barkan, E., 2011. Oxygen isotope fractionation in the ocean surface and 18O/16O of atmospheric O 2. Glob. Biogeochem. Cycles 25. https://doi.org/10.1029/2011GB004178.

Marañón, E., Cermeño, P., Fernández, E., Rodríguez, J., Zabala, L., 2004. Significance and mechanisms of photosynthetic production of dissolved organic carbon in a coastal eutrophic ecosystem. Limnol. Oceanogr. 49, 1652–1666. https://doi.org/10.4319/lo.2004.49.5.1652.

Marra, J., 2009. Net and gross productivity: weighing in with 14C. Aquat. Microb. Ecol. 123–131. https://doi.org/10.3354/ame01306.

Marra, J., 2012. Comment on "Measuring primary production rates in the ocean: enigmatic results between incubation and non-incubation methods at Station ALOHA". In: Quay, P.D., et al. (Eds.), Global Biogeochem Cycles, 26. https://doi.org/10.1029/2011gb004087 n/a-n/a.

Marra, J., Barber, R.T., 2004. Phytoplankton and heterotrophic respiration in the surface layer of the ocean. Geophys. Res. Lett. 31. https://doi.org/10.1029/2004GL019664.

Marra, J.F., Barber, R.T., Barber, E., Bidigare, R.R., Chamberlin, W.S., Goericke, R., Hargreaves, B.R., Hiscock, M., Iturriaga, R., Johnson, Z.I., Kiefer, D.A., Kinkade, C., Knudson, C., Lance, V., Langdon, C., Lee, Z.P., Perry, M.J., Smith, W.O., Vaillancourt, R., Zoffoli, L., 2021. A database of ocean primary productivity from the 14C method. Limnol. Oceanogr. Lett. 6, 107–111. https://doi.org/10.1002/lol2.10175.

Martínez-Vicente, V., Evers-King, H., Roy, S., Kostadinov, T.S., Tarran, G.A., Graff, J.R., Brewin, R.J.W., Dall'Olmo, G., Jackson, T., Hickman, A.E., Röttgers, R., Krasemann, H., Marañón, E., Platt, T., Sathyendranath, S., 2017. Intercomparison of ocean color algorithms for picophytoplankton carbon in the ocean. Front. Mar. Sci. 4. https://doi.org/10.3389/fmars.2017.00378.

Mattei, F., Scardi, M., 2021. Collection and analysis of a global marine phytoplankton primary-production dataset. Earth Syst. Sci. Data 13, 4967–4985. https://doi.org/10.5194/essd-13-4967-2021.

Menden-Deuer, S., Lessard, E.J., 2000. Carbon to volume relationships for dinoflagellates, diatoms, and other protist plankton. Limnol. Oceanogr. 45, 569–579. https://doi.org/10.4319/lo.2000.45.3.0569.

Messié, M., Chavez, F.P., 2015. Seasonal regulation of primary production in eastern boundary upwelling systems. Prog. Oceanogr. 134, 1–18. https://doi.org/10.1016/j.pocean.2014.10.011.

Milligan, A.J., Halsey, K.H., Behrenfeld, M.J., 2015. Advancing interpretations of 14C-uptake measurements in the context of phytoplankton physiology and ecology. J. Plankton Res. 37, 692–698. https://doi.org/10.1093/plankt/fbv051.

Milutinović, S., Bertino, L., 2011. Assessment and propagation of uncertainties in input terms through an ocean-color-based model of primary productivity. Remote Sens. Environ. 115, 1906–1917. https://doi.org/10.1016/j.rse.2011.03.013.

Morán, X.A., Estrada, M., 2001. Short-term variability of photosynthetic parameters and particulate and dissolved primary production in the Alborean Sea (SW Mediterranean). Mar. Ecol. Prog. Ser. 212, 53–67.

Morel, A., 1991. Light and marine photosynthesis: a spectral model with geochemical and climatological implications. Prog. Oceanogr. 26, 263–306. https://doi.org/10.1016/0079-6611(91)90004-6.

Mousseau, L., Dauchez, S., Legendre, L., Fortier, L., 1995. Photosynthetic carbon uptake by marine phytoplankton: comparison of the stable (13C) and radioactive (14C) isotope methods. J. Plankton Res. 17, 1449–1460. https://doi.org/10.1093/plankt/17.7.1449.

Norrman, B., Zwelfel, U.L., Hopkinson, C.S., Brian, F., 1995. Production and utilization of dissolved organic carbon during an experimental diatom bloom. Limnol. Oceanogr. 40, 898–907. https://doi.org/10.4319/lo.1995.40.5.0898.

Olenina, I., Hadju, S., Edler, L., Anderson, A., Wasmund, N., Busch, S., Göbel, J., Gromisz, S., Huseby, S., Huttunen, M., Jeanus, A., Kokkonen, P., Ledaine, I., Niemkiewicz, E., 2006. Biovolumes and Size-Classes of Phytoplankton in the Baltic Sea Helsinki Commission Baltic Marine Environment Protection Commission.

Palevsky, H.I., Quay, P.D., Nicholson, D.P., 2016. Discrepant estimates of primary and export production from satellite algorithms, a biogeochemical model, and geochemical tracer measurements in the North Pacific Ocean. Geophys. Res. Lett. 43, 8645–8653. https://doi.org/10.1002/2016GL070226.

Pauly, D., Christensen, V., 1995. Primary production required to sustain global fisheries. Nature 374, 255–257. https://doi.org/10.1038/374255a0.

Pauly, D., Zeller, D., 2016. Catch reconstructions reveal that global marine fisheries catches are higher than reported and declining. Nat. Commun. 7. https://doi.org/10.1038/ncomms10244.

Platt, T.C., Lewis, M.R., 1987. Estimation of phytoplankton production by remote sensing. Adv. Space Res. 7, 131–135. https://doi.org/10.1016/0273-1177(87)90177-3.

Platt, T., Sathyendranath, S., 1988. Oceanic Primary Production: Estimation by Remote Sensing at Local and Regional Scales, New Series.

Puddu, A., Zoppini, A., Fazi, S., Rosati, M., Amalfitano, S., Magaletti, E., 2003. Bacterial uptake of DOM released from P-limited phytoplankton. In: FEMS Microbiology Ecology. Elsevier, pp. 257–268. https://doi.org/10.1016/S0168-6496(03)00197-1.

Quay, P.D., Peacock, C., Bjrkman, K., Karl, D.M., 2010. Measuring primary production rates in the ocean: Enigmatic results between incubation and non-incubation methods at Station ALOHA. Glob. Biogeochem. Cycles 24. https://doi.org/10.1029/2009GB003665.

Regaudie-de-Gioux, A., Lasternas, S., Agustí, S., Duarte, C.M., 2014. Comparing marine primary production estimates through different methods and development of conversion equations. Front. Mar. Sci. 1. https://doi.org/10.3389/fmars.2014.00019.

Regaudie-de-Gioux, A., Huete-Ortega, M., Sobrino, C., López-Sandoval, D.C., González, N., Fernández-Carrera, A., Vidal, M., Marañón, E., Cermeño, P., Latasa, M., Agustí, S., Duarte, C.M., 2019. Multi-model remote sensing assessment of primary production in the subtropical gyres. J. Mar. Syst. 196, 97–106. https://doi.org/10.1016/j.jmarsys.2019.03.007.

Robinson, C., Tilstone, G.H., Rees, A.P., Smyth, T.J., Fishwick, J.R., Tarran, G.A., Luz, B., Barkan, E., David, E., 2009. Comparison of in vitro and in situ plankton production determinations. Aquat. Microb. Ecol. 54, 13–34. https://doi.org/10.3354/ame01250.

Ryther, J.H., 1956. Photosynthesis in the ocean as a function of light intensity. Limnol. Oceanogr. 1, 61–70. https://doi.org/10.4319/lo.1956.1.1.0061.

Ryther, J.H., Yentsch, C.S., 1957. The estimation of phytoplankton production in the ocean from chlorophyll and light data. Limnol. Oceanogr. 2, 281–286. https://doi.org/10.1002/lno.1957.2.3.0281.

Saba, V.S., Friedrichs, M.A.M., Antoine, D., Armstrong, R.A., Asanuma, I., Behrenfeld, M.J., Ciotti, A.M., Dowell, M., Hoepffner, N., Hyde, K.J.W., Ishizaka, J., Kameda, T., Marra, J., Mlin, F., Morel, A., O'Reilly, J., Scardi, M., Smith, W.O., Smyth, T.J., Tang, S., Uitz, J., Waters, K., Westberry, T.K., 2011. An evaluation of ocean color model estimates of marine primary productivity in coastal and pelagic regions across the globe. Biogeosciences 8, 489–503. https://doi.org/10.5194/bg-8-489-2011.

Sanz-Martín, M., Vernet, M., Cape, M.R., Cano, E.M., Delgado-Huertas, A., Reigstad, M., Wassmann, P.F., Duarte, C.M., 2019. Relationship between carbon- and oxygen-based primary productivity in the Arctic Ocean, svalbard archipelago. Front. Mar. Sci. 6. https://doi.org/10.3389/fmars.2019.00468.

Sathyendranath, S., Stuart, V., Nair, A., Oka, K., Nakane, T., Bouman, H., Forget, M.H., Maass, H., Platt, T., 2009. Carbon-to-chlorophyll ratio and growth rate of phytoplankton in the sea. Mar. Ecol. Prog. Ser. 383, 73–84. https://doi.org/10.3354/meps07998.

Siegel, D.A., Westberry, T.K., O'brien, M.C., Nelson, N.B., Michaels, A.F., Morrison, J.R., Scott, A., Caporelli, E.A., Sorensen, J.C., Maritorena, S., Garver, S.A., Brody, E.A., Ubante, J., Hammer, M.A., 2001. Bio-optical modeling of primary production on regional scales: the Bermuda BioOptics project. Deep-Sea Res. II 48, 1865–1896.

Silsbe, G.M., Behrenfeld, M.J., Halsey, K.H., Milligan, A.J., Westberry, T.K., 2016. The CAFE model: a net production model for global ocean phytoplankton. Glob. Biogeochem. Cycles 30, 1756–1777. https://doi.org/10.1002/2016GB005521.

Slawyk, G., Collos, Y., Auclair, J.-C., 1977. The use of the 13C and 15N isotopes for the simultaneous measurement of carbon and nitrogen turnover rates in marine phytoplankton. Limnol. Oceanogr. https://doi.org/10.4319/lo.1977.22.5.0925.

Steeman-Nielsen, E., 1952. The use of radio-active carbon (C14) for measuring organic production in the sea. ICES J. Mar. Sci. 18, 117–140. https://doi.org/10.1093/icesjms/18.2.117.

Trentman, M.T., Hall, R.O., Valett, H.M., 2023. Exploring the mismatch between the theory and application of photosynthetic quotients in aquatic ecosystems. Limnol. Oceanogr. Lett. 8, 565–579. https://doi.org/10.1002/lol2.10326.

Utermöhl, H., 1931. Neue Wege in der quantitativen Erfassung des Plankton. (Mit besonderer Berücksichtigung des Ultraplanktons.). SIL Proc. 5, 567–596. https://doi.org/10.1080/03680770.1931.11898492.

Westberry, T.K., Behrenfeld, M.J., 2014. Oceanic net primary production. In: Hanes, J.M. (Ed.), Biophysical Applications of Satellite Remote Sensing. Springer Berlin Heidelberg, Berlin, Heidelberg, pp. 205–230. https://doi.org/10.1007/978-3-642-25047-7_8.

Westberry, T., Behrenfeld, M.J., Siegel, D.A., Boss, E., 2008. Carbon-based primary productivity modeling with vertically resolved photoacclimation. Glob. Biogeochem. Cycles 22. https://doi.org/10.1029/2007GB003078.

Westberry, T.K., Silsbe, G.M., Behrenfeld, M.J., 2023. Gross and net primary production in the global ocean: an ocean color remote sensing perspective. Earth Sci. Rev. https://doi.org/10.1016/j.earscirev.2023.104322.